Article

Not peer-reviewed version

40-Year Fire History Reconstruction from Landsat Data in a Mediterranean Area of North Africa Following International Standards

Mostefa E. Kouachi , Amin Khairoun , Aymen Moghli , Souad Rahmani , Florent Mouillot , M. Jaime Baeza , Hassane Moutahir *

Posted Date: 3 April 2024

doi: 10.20944/preprints202404.0307.v1

Keywords: Algeria; BA products; Mediterranean Basin; Landsat; BAMTs; Google Earth Engine.

Article

40-Year Fire History Reconstruction from Landsat Data in a Mediterranean Area of North Africa Following International Standards

Mostefa E. Kouachi [1,2], Amin Khairoun [3], Aymen Moghli [4,5], Souad Rahmani [6], Florent Mouillot [7], M. Jaime Baeza [1] and Hassane Moutahir [1,8,*]

[1] Department of Ecology, University of Alicante, 03690 San Vicente del Raspeig, Alicante, Spain; mek12@alu.ua.es
[2] Forests Conservation of Sétif, Directorate General of Forests (DGF), Cité Ain Tbinet 19000, Sétif, Algeria; mek12@alu.ua.es
[3] University of Alcalá, Environmental Remote Sensing Research Group, Department of Geology, Geography and the Environment, Colegios 2, 28801, Alcalá de Henares, Spain; amin.khairoun@uah.es
[4] Department of Biology and Plant Ecology, Faculty of Nature and Life Sciences, University of Sétif 1, Campus El-Bez, Algiers Road, Sétif 19137, Algeria; moghliaymen@gmail.com
[5] Forest Sciences and Technology Centre of Catalonia, Solsona, Spain; moghliaymen@gmail.com
[6] Department of Ecology and Environment, Faculty of Nature and Life Sciences, University of Batna 2, 53 Constantine Road, Fesdis 05078, Batna, Algeria; s.rahmani@univ-batna2.dz
[7] Centre d'Ecologie Fonctionnelle et Evolutive CEFE, UMR 5175, CNRS, Université Paul-Valéry Montpellier, EPHE, IRD, 1919 Route de Mende, 34293 Montpellier Cedex 5, France; florent.mouillot@cefe.cnrs.fr
[8] Institute of Meteorology and Climate Research (IMK-IFU), Karlsruhe Institute of Technology, Campus Alpin, Kreuzeckbahnstraße 19, 82467 Garmisch-Partenkirchen, Germany; hassane.moutahir@kit.edu
* Correspondence: hassane.moutahir@kit.edu

Abstract: Algeria, the main fire hotspot on the southern rim of the Mediterranean Basin, lacks complete fire dataset with official fire perimeters, and the existing one contains inconsistencies. Preprocessed global and regional burned area (BA) products provide valuable insights into fire patterns, characteristics and dynamics over time and space, and into their impact on climate change. Nevertheless, they exhibit certain limitations linked with their inherent spatio-temporal resolutions. To address the need for reliable BA information in Algeria, we systematically reconstructed, validated and analyzed a 40-year (1984–2023) BA product (NEALGEBA; North Eastern ALGeria Burned Area) at 30-m spatial resolution in the typical Mediterranean Ecosystems of this region, following international standards. We used Landsat data and the BA Mapping Tools (BAMTs) in the Google Earth Engine (GEE) to map BAs. The spatial validation of NEALGEBA, performed for 2017 and 2021 using independent 10-m spatial resolution Sentinel-2 reference data, showed overall accuracies > 98.10 %; commission and omission errors < 8.20 %; Dice coefficients > 91.90 %, and relative biases < 3.44 %. The temporal validation, however, using MODIS and VIIRS active fire hotspots, emphasized the limitation of Landsat-based BA products in temporal fire reporting accuracy terms. The intercomparison with five readily available BA products for 2017, by using the same validation process, demonstrated the overall outperformance of NEALGEBA. Furthermore, our BA product exhibited the highest correspondence with the ground-based BA estimates. NEALGEBA currently represents the most extensive and reliable time series of BA history at fine spatial resolution for NE Algeria, offering a significant contribution for further national and international fire hazard and impact assessments and acts as a reference dataset for contextualizing future weather extremes, such as the 2023 exceptional heat wave, which we show not to have led to the most extreme fire year over the last four decades.

Keywords: Algeria; BA products; mediterranean basin; landsat; BAMTs; google earth engine

 doi:10.20944/preprints202404.0307.v1

1. Introduction

Fire is an intrinsic process of the Earth system [1], which is projected to increase in burned areas (BAs) owing to climate change and escalating anthropogenic effects [2]. Among all forest disturbances, fire is the major forest destructive agent in the Mediterranean Basin [3], where heat wave-related fires may increase in the future [4]. When looking across the African side of the Mediterranean Basin, Algeria is the main fire hotspot [5]. Throughout history, this country has witnessed an unprecedented series of large extreme fires [6], with a record-breaking heatwave in the summer of 2023, which affected ecological and socio-economic assets [7,8], including human casualties. These fires may seriously degrade forest habitats in this country, a large part of which may not be restored [9]. However, accurate and spatially explicit BA data about this region, as in several middle-eastern and north-African countries, are scarce or even lacking [10].

Remote sensing has become the most efficient tool for addressing all fire management aspects, including the generation of BA products [11]. Unlike ground-based fire datasets that are often biased or incomplete, or exhibit inconsistencies [12–14], satellite-derived BA products provide spatially and temporally consistent and reliable information about fires on regional and global scales [15]. In practice, several pixel-level BA products have been employed in a wide range of research works, including global fire trends [16], characterization of fire regimes [17,18], climate impact on fire patterns [19], fire emission modelling [20] and fire model benchmarking [21], and to derive global databases of single fire events [22].

Early global BA products were based on the coarse resolution data from the SPOT-VGT, ERS2-ATSR2, ENVISAT-AATSR, NOAA-AVHRR, PROBA-V and MODIS sensors [15]. In the last few years, major efforts have been made to develop comprehensive global and regional BA products, mainly according to two major programs: the ESA Fire Disturbance Climate Change Initiative (FireCCI) and the NASA MODIS Land Science Team. The current global BA products from the ESA FireCCI project include: FireCCI51 (2001–2020; 250 m), which derives from the MODIS surface reflectance imagery coupled with thermal anomaly observations [23]; FireCCILT11 (1982–2018; 5 km) from AVHRR LTDR [24], including new developments and sensors as in FireCCIS310 (2019; 300 m) from Sentinel-3 SYN coupled with VIIRS active fire hotspots [25]. Perspectives with newly delivered medium-resolution sensors have been tested regionally, such as FireCCISFD11 and FireCCISFD20 (2016 and 2019, respectively; 20 m) from the Sentinel-2 MSI coupled with the active fire data for sub-Saharan Africa [26,27]. On the other hand, the MCD64A1 collection 6.1 (2000–present; 500 m) is NASA's current standard global BA product, which derives from MODIS daily surface reflectance imagery combined with MODIS active fire data [28].

Other available coarse-resolution products from different agencies include the Copernicus Climate Change Service Burned Area product, version 1.1 (C3SBA11) (2017–2022; 300 m) from Sentinel-3 OLCI data [29] and the European Forest Fire Information System (EFFIS) BA product (2000–present; 250 m and 20 m) from the MODIS and Sentinel-2 imagery [30]. Additional efforts have been made to provide finer-resolution BA products, a major end-user request [31]. Landsat-based BA mapping includes the novel 30-m resolution Global Annual Burned Area Maps (GABAM 1985–2019; 30 m), which derived from the Landsat dense time-series data by means of a global automated BA mapping approach [32] in the Google Earth Engine (GEE) [33]. In the same context, albeit with limited spatial coverage, other products include the Monitoring Trends in Burn Severity (MTBS 1984–2022; 30 m) across the whole of the U.S. [34], and the Landsat Collections 1 and 2 BA products for CONUS (1984–2022; 30 m) [35].

Although freely accessible for the scientific community with widespread use on different spatial and temporal scales, the above-mentioned BA products exhibit certain limitations. These are mainly caused by the inherent coarse spatial resolution that results in very high omission rates of small burned patches [26,27,36,37], particularly in the Mediterranean Basin where smaller fires happen [10,38], poor temporal fire reporting accuracy to prevent a fire seasonality analysis [32], and limited spatial and temporal coverage [34,35], which restrict their usage in other areas of the globe.

In Algeria, the available ground-based fire dataset provides invaluable information that can hardly be obtained by satellite-based systems. This includes, among others, the exact date and time

 doi:10.20944/preprints202404.0307.v1

of ignition/intervention/extinction, burned vegetation type and species, origin, and cause of fires. Nevertheless, this dataset is acknowledged to be incomplete, lacks fire perimeters and displays discrepancies in fire extent terms. This is attributed mainly to the visual estimation of fire-affected areas, which is often conservative especially in inaccessible areas. Furthermore, a standardized BA estimation protocol across local forest services in the country is lacking.

Considering these limitations in both national statistics and the performance of existing BA datasets, the development of a reliable and long-term BA product for such an insufficiently investigated part of the Mediterranean Basin would strengthen future research into forest management plans and for understanding Mediterranean fire hazards in this southern part of the Mediterranean Basin [5,13]. This would allow accurate in-depth analyses of the fire regime over lengthy time periods, and to learn the factors that underlie fire occurrence and propagation in this region with a Mediterranean climate, but with substantial socio-economic and political differences compared to the more studied European side of the Mediterranean Basin.

In recent years, several BA-mapping approaches have been developed for different study regions using medium-resolution data [39–41], including the BA Mapping Tools (BAMTs) [42]. By leveraging the powerful capabilities of the GEE's cloud computing platform [33], the BAMTs constitute not only a significant stride as innovative, time-efficient, and resource-conserving tools for accurate multi-year BA mapping [10,43], but also the creation of independent reference data for validation exercises [44–46].

Based on these premises, we aim to exploit these efficient tools for systematically reconstructing the fire history in NE Algeria. Specifically, we aim to: (1) generate a BA product from the Landsat Collection-2 Surface Reflectance (LC2SR) product covering the 1984–2023 period; (2) assess its spatio-temporal consistency; (3) provide pieces of evidence for a significantly revised BA estimate compared to existing BA products (GABAM, FireCCI51, C3SBA11, MCD64A1, and EFFIS) and a ground-based fire dataset. This work constitutes the mandatory initial step for creating a spatially explicit BA database following international standards for the whole of Algeria to further open a major research field for fire hazard, impacts and vulnerability assessments that lead to firefighting and fire management policies [47].

2. Materials and Methods

2.1. Study Area

The study area is located in NE Algeria, on the southern rim of the Mediterranean Basin, and spans longitudes from 3.71° E to 8.68° E and latitudes from 36.21° N to 37.08° N. The total study area covers 17,036 km^2. It includes the coastal "Wilayas" (administrative provinces) of Annaba, Béjaïa, El-Tarf, Jijel, Skikda, and Tizi Ouzou in a narrow strip that stretches 440 km in length and up to 96 km in depth, with altitudes ranging from m.s.l. to 2 291 m (Figure 1a and b). Landscapes are typically Mediterranean dominated by forests, shrubs, and grasslands, where the mean annual rainfall varies from 725 to 924 mm (Figure 1c and Table 1). The main forest types are composed of oaks, such as cork-oak (*Quercus suber* L.), Algerian oak (*Quercus canariensis* Willd.), African oak (*Quercus afares* Pomel.) and holm oak (*Quercus ilex* L.), and of conifers, such as maritime pine (*Pinus pinaster* Aiton.), Aleppo pine (*Pinus halepensis* Miller.), and Atlas cedar (*Cedrus atlantica* (Endl.) Carrière.). Our study area is acknowledged as being one of the regional plant biodiversity hotspots in the Mediterranean Basin [48]. It harbors the densest, richest, and most pristine forest ecosystems, which are reflected in four National Parks (Djurdjura, Gouraya, Taza and El-Kala) that form part of the UNESCO World Network of Biosphere Reserves (WNBR) [49]. However, this region experiences the highest incidence of fires in the country [50,51] owing to high fuel availability, extreme climate conditions in summer (prolonged drought and Saharan heat waves), and increasing anthropogenic activities [5].

Preprints.org (www.preprints.org) | NOT PEER-REVIEWED | Posted: 3 April 2024 doi:10.20944/preprints202404.0307.v1

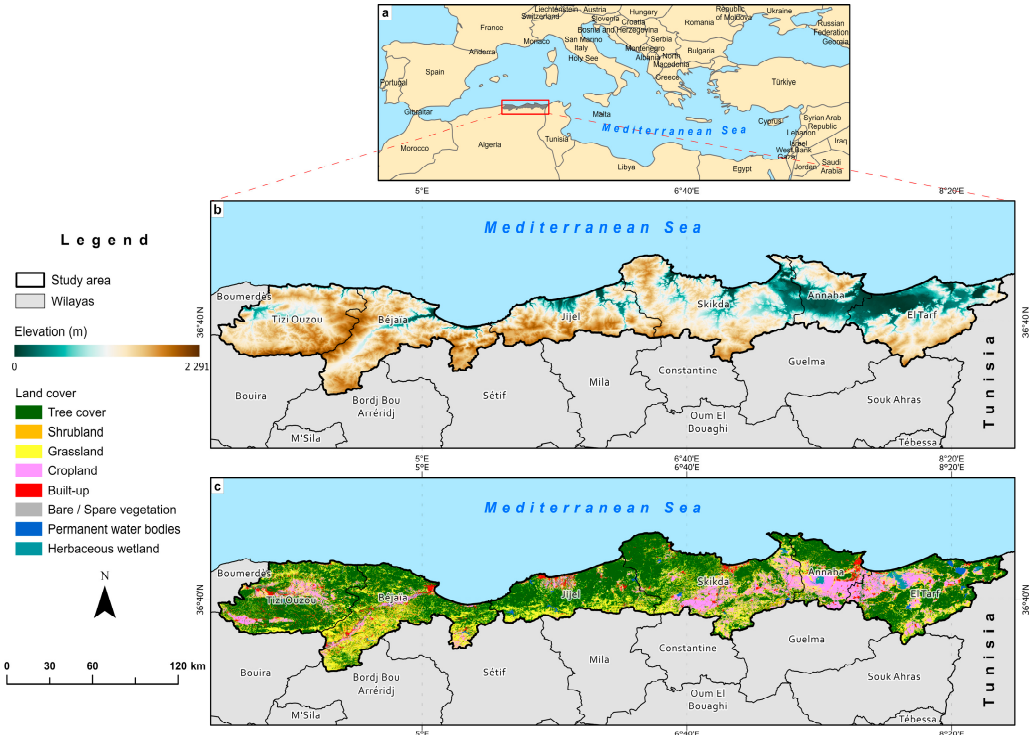

Figure 1. (**a**) Location of the study area (NE Algeria) in the Mediterranean Basin; (**b**) Land use cover (source: © ESA WorldCover project 2021/Contains modified Copernicus Sentinel data (2021) processed WorldCover consortium [52]), and (**c**) Elevation (source: Shuttle Radar Topography Mission (SRTM) 1 Arc-Second Global [53]).

Table 1. Total land area and natural vegetation type areas and mean annual rainfall (P) in the six studied wilayas.

Wilayas	Area (km²)	Natural vegetation areas (km²) *			Natural vegetation/Wilaya	P (mm) **
		Tree cover	Shrubland	Grassland		
Annaba	1 411.52	609.40	80.74	235.47	0.66	825
Béjaïa	3 226.11	1 434.69	278.52	1 138.15	0.88	767.6
El-Tarf	2 885.32	1 420.59	157.65	601.80	0.76	792.6
Jijel	2 397.22	1 437.11	61.75	693.88	0.91	924.1
Skikda	4 146.60	1 924.21	295.43	1 096.41	0.80	725
Tizi Ouzou	2 969.21	1 661.12	133.80	727.29	0.85	913

* Based on the ESA WorldCover 2021 map [52], ** data from the National Meteorological Office (ONM).

2.2. Input Data

2.2.1. Landsat and Sentinel-2 Imagery

The NASA/USGS Landsat program has launched eight Earth Observation (EO) satellites to date. These satellites have been continuously collecting data on the Earth's land surface for over 50 years, the world's longest EO data series (1972–present-day) [54]. Different multispectral and thermal sensors have been developed, including Landsat 1–5 MSS (1972–1999), Landsat-4 TM (1982–1993), Landsat-5 TM (1984–2012), Landsat-7 ETM+ (1999–2021), and the currently operational Landsat-8 OLI/TIRS (2013–present-day) and Landsat-9 OLI-2/TIRS-2 (2021–present-day) [55]. Landsat instruments from TM to OLI-2/TIRS-2 eras have been generating scenes over 185 km swath width using the Worldwide Reference System-2 (WRS-2) with seven, eight and 11 spectral bands at 15 m (panchromatic), 30 m (visible, NIR, SWIR, coastal/aerosol, and cirrus), and 60–120 m (thermal bands) spatial resolutions every 16 days, reduced to 8 days when two satellites are combined (currently,

 doi:10.20944/preprints202404.0307.v1

Landsat 8 and 9). The ESA/Copernicus Sentinel-2 Mission comprises a constellation of two identical EO satellites, Sentinel-2A and 2B, which have been simultaneously orbiting the Earth since July 2015 and July 2017, respectively. The Sentinel-2 MSI sensor captures scenes of 110 × 110 km² using the Military Grid Reference System (MGRS) with 13 spectral bands at 10 m (visible and NIR), 20 m (red edge and SWIR) and 60 m (atmospheric bands) every 10 days, or every 5 days with both satellites combined [56]. In this work, we used the LC2SR images from the last five Landsat satellites (1984–2023) and Sentinel-2 Level-1C Top of Atmosphere (TOA) reflectance images (2017 and 2021), both available as image collections in the Earth Engine Data Catalogue (EEDC) (https://developers.google.com/earth-engine/datasets, last accessed December 2023).

2.2.2. Global Burned Area Products

To evaluate our generated BA product, we made a comparison to different existing BA products. For this purpose, we used five readily available BA products with different spatial resolutions:

1. The GABAM is the first and only medium-resolution BA product at 30-m resolution with a global scale and long-term BA data to date. A novel automatic pipeline [32] was applied to generate the annual global BA maps from the Landsat time-series on the GEE platform [33] from 1985 to 2019. Nevertheless, 1986, 1988, 1990, 1991, 1993, 1994, 1997 and 1999 are unavailable. Yearly GABAM composites were downloaded as 10° × 10° tiles in GeoTIFF format at ftp://124.16.184.141/GABAM (accessed February 2023).
2. The FireCCI51 provides monthly global BA maps at the 250-m spatial resolution based on a hybrid algorithm coupling daily surface reflectance imagery and the active fire data from MODIS for 2001–2020 [23]. The FireCCI51 pixel product in GeoTIFF format was downloaded at https://doi.org/10.5285/58f00d8814064b79a0c49662ad3af537 (accessed April 2023).
3. The C3SBA11 delivers monthly global BA maps at 300-m spatial resolution since 2017 onwards, using an adaptation of the FireCCI51 BA algorithm to Sentinel-3 OLCI data [25]. The pixel BA product was obtained from the C3S Climate Data Store (CDS) in NetCDF files at https://doi.org/10.24381/cds.f333cf85 (accessed April 2023).
4. The MCD64A1 collection 6.1 BA mapping approach combines daily surface reflectance images with the active fire data from MODIS to produce monthly global BA maps at a spatial resolution of 500 m from 2000 onwards [28]. The product is provided by the USGS Land Processes Distributed Active Archive Centre (LP-DAAC) and was obtained in GeoTIFF format from the Application for Extracting and Exploring Analysis Ready Samples (AppEEARS) service (https://lpdaacsvc.cr.usgs.gov/appeears/, accessed April 2023).
5. The EFFIS BA product provides daily updates of fire contours with information on the initial and final dates of burn detection, BAs, administrative units, and vegetation type for 49 countries in Europe, the Middle East, and North Africa (MENA) from 2000 to the present-day. The EFFIS Rapid Damage Assessment (RDA) module performs BA delineation by processing daily imagery from the MODIS instrument at a spatial resolution of 250 m [30]. Since 2018, EFFIS fire contours have been generated using the 20-m resolution Sentinel-2 imagery. For Algeria, EFFIS fire contours are available only for 2004 and 2005, and from 2009 onwards. The EFFIS BA product was provided in the ESRI Shapefile format from the EFFIS of the European Commission Joint Research Centre (https://effis.jrc.ec.europa.eu, accessed April 2023).

2.2.3. Active Fire Products

Active fire observations from the MODIS and VIIRS sensors were leveraged to examine the temporal fire reporting accuracy of our BA product by comparing detected burn dates to active fire dates. In line with this, the standard MCD14ML collection 6.1 product from MODIS onboard Terra and Aqua provides the systematic detection of active fires worldwide at 1-km resolution from November 2000 to the present-day [57]. In contrast, the 375 m standard VIIRS VNP14IMGML collection 1 product offers better accuracy in detecting active fires from January 2012 onwards [58]. These datasets were provided as feature point data in the ESRI Shapefile format by the Fire

 doi:10.20944/preprints202404.0307.v1

Information for Resource Management System (FIRMS) (https://firms.modaps.eosdis.nasa.gov/download/, accessed January 2024).

2.2.4. Ground-Based Fire Dataset

Ground-based annual BA estimates over the 1985–2023 period for the six wilayas under study were provided by the Directorate General of Forests (DGF), which operates under the authority of the Algerian Ministry of Agriculture and Rural Development (MADR), Algeria. The DGF oversees fire prevention and control, and develops national strategies and action plans for fire management across the country. Fire statistics are collected from 40 local forest services of the different wilayas that are regularly affected by fires [50]. However, detailed single-fire datasets have been recently compiled only for the 2012–2023 period, where detailed information is provided: smallest administrative division, forest name or locality, latitudes/longitudes, date and time of ignition/intervention/extinction, burned vegetation type, and more. Here we note that the minimum recorded fire size is not standardized across years and wilayas, a common feature that has been previously reported in Spain [59], France [60] or Tunisia [13], for which a standard threshold of 0.1 ha is usually assumed.

2.2.5. Land Cover Map

The ESA WorldCover project produced 10 m resolution global land cover maps for 2020 and 2021 from Sentinel-1 and Sentinel-2 data with 11 land cover classes conforming to the UN-FAO's Land Cover Classification System (LCCS) [52]. We obtained the GeoTIFF land cover map of 2021 for our study area from ESA at https://worldcover2021.esa.int/downloader (accessed May 2023).

2.3. Burned Area Generation

In 2014, Bastarrika et al. [61] developed a Landsat interactive BA mapping procedure, named the BA Mapping Software (BAMS). This software allowed to supervise the BA mapping between single pre- and postfire images by adopting a two-phase supervised strategy [62]. This approach has been widely employed to create fire reference perimeters to validate global and regional BA products [23,26,27,63–65], and to operationally reconstruct historical fires in Greece (1984–1991 and 1999–2011) [66], Argentina (1999–2011) [67] and Tunisia (1984–2010) [13]. However, it heavily depended on the system's computational capacity and had several limitations, including the inability to work with higher resolution Sentinel-2 data and maintenance difficulties due to changes in the Landsat data format and metadata, which led to frequent malfunctioning and uncontrolled commissions over agricultural and cloud-shadowed areas [42]. To address these limitations, Roteta et al. [42] proposed the BA Mapping Tools (BAMTs). The current version (BAMTs v1.7) presents a set of six tools implemented in the GEE [33] that perform BA mapping (BA Cartography tool), the selection of validation areas (VA tool) and image dates (VA Dates tool), reference data creation (RP tool), validation (Assessment tool) and image data visualization (Image Viewer). The JavaScript API scripts for these tools with a user guide are publicly available at https://github.com/ekhiroteta/BAMT (accessed December 2023).

To generate our BA product, yearly pre- and postfire consecutive multitemporal composites were derived using 10,406 surface reflectance images from the LC2SR product from 1984 to 2023 with the BA Cartography tool to cover the whole study area. This tool is a semi-automatic BA algorithm that performs the supervised classification of Landsat or Sentinel-2 data based on a Random Forest (RF) machine-learning classifier [68]. For each year, the prefire period was defined from January 1st to April 30th, and the postfire period from May 1st to December 31st, following Roteta et al. [42]. This was done to employ the maximum number of cloud-free scenes and to, thus, reduce BA omissions, and to capture all the fires with detection delays caused by the Landsat revisit time (8–16 days).

In addition to six reflectance bands over the visible near-infrared (VNIR) and short-wavelength infrared (SWIR), for each Landsat image during the pre- and postfire periods, the BA Cartography tool computes three spectral indices: the normalized difference vegetation index (NDVI) [69]; the

 doi:10.20944/preprints202404.0307.v1

normalized burn ratio (NBR) [70]; the normalized burn ratio 2 (NBR2) [71]. The date with the lowest NBR value (date of the strongest burn signal) was used to generate image mosaics. Then a difference image was generated by subtracting the post- and prefire image composites. Subsequently, the RF classifier was iteratively trained using burned and unburned polygons, which were defined incrementally over both temporal composites until the desired BA delineation accuracy was achieved. On average, 38,894 burned and 45,723 unburned training samples (pixels) were manually and visually delineated every year. In the BA cartography tool, a shapefile vector layer was used as a mask to limit the processing extent to our study area. The RF model is widely applied for BA extractions from medium-resolution data [32,46]. Next, a two-phase supervised strategy to balance errors of commission and omission [61,62] was employed on the RF probability Images. In the first phase, seed pixels with strong burned signals were extracted using a threshold based on the average probabilities of the burned training samples. In the second phase, a region-growing process was applied up to a 50% threshold outwardly from the seed pixels to capture the entire burned patch using Rook's case contiguity, where only the burned patches containing at least one seed pixel were labelled as burned.

Finally, each annual BA map was exported as four 2° × 2° tiles at the 30-m resolution in the ESRI Shapefile format, and a thorough fire-by-fire interactive visual quality check was performed in a GIS environment to ensure the highest quality of the final burned patches. This allowed a few anomalies to be eliminated, such as very few continuous strip lines (one to two pixels wide), often starting from the edge of detected burned patches. These errors are caused mainly by the Landsat-7 ETM+ SLC failure. Each burned polygon has a single attribute: indicating either the approximate burn detection date or null values for unobserved areas (i.e., clouds and cloud shadows).

At this step, it is important to note that the supervised BA contouring process under the BA Cartography tool may not be accomplished because of GEE's scaling errors [42]. This issue was specifically encountered with years holding large amounts of BA. To avoid this shortcoming, we opted for a balanced and conservative approach when training the burned/unburned samples by avoiding very large polygons and complex geometries. The procedural steps for the generation and validation of the BA product (Phase I and II), and the intercomparison analysis (Phase III) are given in Figure 2.

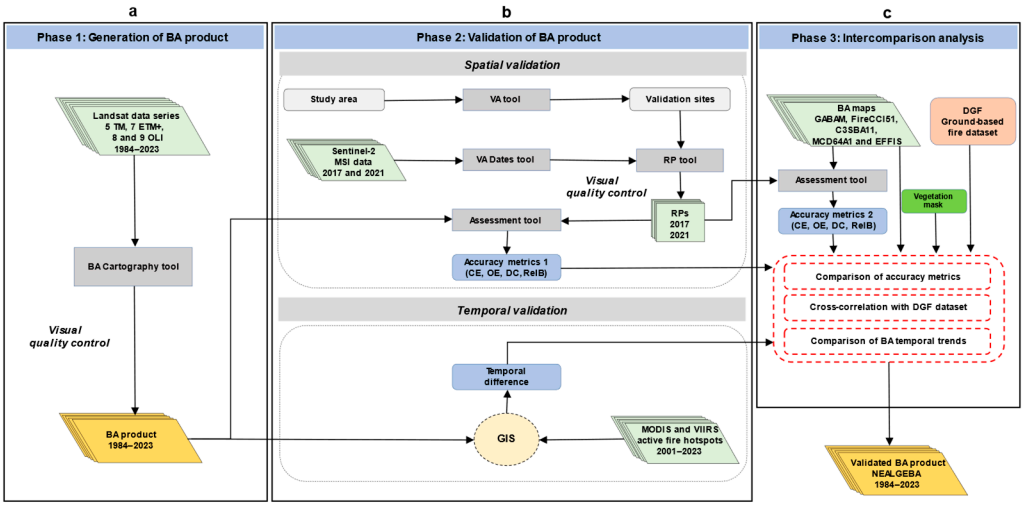

Figure 2. Flow diagram of the procedural steps of the methodology. Generation of the BA product (a), spatio-temporal validation of the generated BA product (b), and intercomparison analysis (c). RPs: Reference Perimeters, CE: Commission Error, OE: Omission Error, OA: Overall Accuracy, DC: Dice coefficient and RelB: Relative Bias.

 doi:10.20944/preprints202404.0307.v1

2.4. Spatio-Temporal Validation

2.4.1. Spatial Validation

Validation plays a pivotal role in ensuring the integrity and reliability of satellite-derived BA products. The Committee on Earth Observation Satellites (CEOS) Working Group on Calibration and Validation (WGCV) defines validation as "the process of assessing, by independent means, the quality of the data products derived from those system outputs" [72]. The spatial validation of our BA product was performed using two validation years: 2017 and 2021. These years were selected because they hold the largest annual BA during Sentinel-2 era (2015–present). Sentinel-2 data are used in Section 2.4.3 below to create independent reference data. To assess the temporal fire reporting accuracy of the BA product, we compared the burn detection dates from the BA Cartography tool to the active fire dates from MODIS and VIIRS.

Five validation areas were sampled for 2017 and 2021 by the VA tool by following a stratified random sampling methodology [73,74]. At each sampling unit, this tool incorporates two key stratification criteria: the predominant Olson biomes [75] and fire activity according to FireCCI51 or MCD64A1. To ensure comprehensive and robust validation, long sampling units (LUs) lasting 100 days, and consisting of 110 × 110 km² tiles with a minimum temporal frequency of 30 days between consecutive Sentinel-2 images and cloud cover below 10%, were employed. This approach ensures a long data series with frequently available cloud-free images to create reliable reference data from the continuous and frequent ground observations throughout validation years. As the generation of high-quality reference data in validation areas of 110 × 110 km² (~ 12 000 km²) is time-intensive, the VA tool was designed to create smaller sampling units at the center of each Sentinel-2 tile [23,27,46,64,76]. However, this subsampling resulted in sampling units not being representative across the study area. To solve this problem, we manually generated a tessellated grid with 168 cells of 20 × 20 km² (400 km²) over the originally sampled validation areas [77]. Thereafter, we selected the cells with the greatest fire activity based on the BA estimates from FireCCI51 in the corresponding validation years. In all, 10 cells were selected as new validation sites, with two cells assigned to each sampled Sentinel-2 tile, and all of them lying in the Mediterranean forest biome (Figure 3).

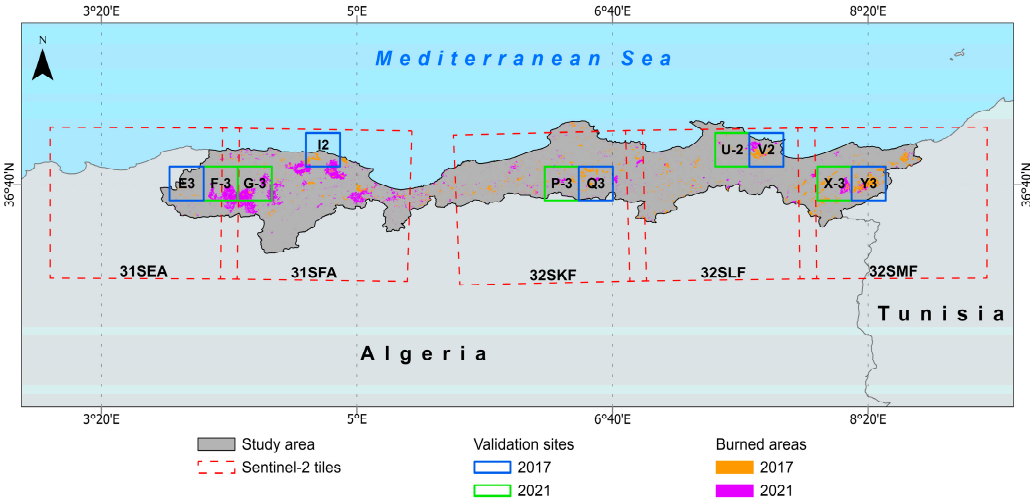

Figure 3. Spatial distribution of the 10 newly sampled validation sites (20 × 20 km²) in the five originally sampled Sentinel-2 tiles (110 × 110 km²) for validation years 2017 and 2021.

To properly date the validation period, the CEOS Land Product Validation Subgroup (CEOS-LPVS) recommends generating reference data from multitemporal pairs of images rather than from single pairs of pre- and postfire images [42,76]. Therefore, 227 Sentinel-2 consecutive images with cloud cover below 10% were identified for each validation site using the VA Dates tool. Validation periods were about 5–7 months for 2017 and 4–8 months for 2021 (Table A1).

 doi:10.20944/preprints202404.0307.v1

Satellite-derived BA product validation requires independent reference data at a higher spatial resolution than the product to be validated [78]. Accordingly, the RP tool was used to extract the 10-m resolution reference perimeters (RPs) from the selected pairs of consecutive Sentinel-2 images at each validation site. The RP tool performs the same BA mapping exercise as the BA Cartography tool, previously used in Section 2.3, albeit with some modifications. Instead of temporal composites, single-image pairs from the pre- and postfire periods were employed. Additionally, the SLC image or QA60 and B1 bands were used to mask clouds and cloud shadows. Likewise, the RF classifier was iteratively trained by defining burned and unburned training pixels until the optimal delineation of burned patches was achieved.

It is important to note that the "cloud cover" information used by the VA Date tool to select the cloud-free Sentinel-2 images at each validation site is that of the entire Sentinel-2 scene (110 x 110 km^2) stored in the image metadata rather than being specific to the manually sampled validation sites (20 x 20 km^2). Consequently, very few consecutive dates were excluded in the reference data creation step owing to high cloud cover that obstructed ground observations. The resulting Sentinel-2 reference data (hereinafter referred to as "S2RD") were exported in the ESRI Shapefile format. A single attribute is given to the S2RD vector layers to indicate burned and unobserved polygons. Finally, a visual quality control of the short units of the RPs was performed before merging them into long units at each validation site [46,76,79] (Figure A1 and Figure A2).

At each validation site, the 2017 and 2021 BA maps were compared to their counterparts from S2RD. The commission error (CE), omission error (OE), overall accuracy (OA), Dice coefficient (DC) [80], and Relative bias (RelB) were computed employing the assessment tool based on the confusion matrix [81]. These accuracy metrics are widely used to assess the accuracy of satellite-derived BA products [45,79,82]. We considered additional metrics to measure the total area correctly detected as burned (SurfBA) or unburned (SurfUB). Similarly, SurfCE and SurfOE represent the total committed and omitted burned surfaces, respectively.

2.4.2. Temporal Validation

The burn detection dates in the BAMTs-derived product were determined based on the most frequently occurring date (the mode) for all the pixels in each detected burned patch in the Landsat post-fire composite [42]. Consequently, these dates do not imperatively correspond to the effective burn dates. To assess our BA product's temporal reporting accuracy, the temporal delay in days was measured between the burn detection dates and the active fire dates from the MODIS and VIIRS hotspots [26,27,46]. Nevertheless, this analysis was performed by bearing in mind all the burned patches in the entire study area for a temporal validation period spanning from 2001 to 2023 rather than at the validation sites because taking specific years as the number of burned patches to be compared was insufficient. To accomplish this, 1 × 1 km^2 windows were created around the yearly active fire hotspots from MCD14ML from 2001 to 2011, which represents the approximate MODIS pixels. Similarly, windows of 375 × 375 m^2 were defined around the VNP14IMGML hotspots from 2012 to 2023. Next, we extracted the most frequent dates from the active fire windows that intersected the individual burned patches in the corresponding years then we compared them to the burn detection dates (Figure A3).

This analysis was performed on 33.68% of the burned patches (n = 22,236), which represented the intersection rate with the active fire windows from MODIS and VIIRS. Burned patches were found in 49.14% of the active fire windows (n = 9,030 from MCD14ML and n = 34,745 from VNP14IMGML) between 2001 and 2023. The remaining burned patches (66.32%) were not found in the active fire windows, which can be explained by active fire sensors' native coarse spatial resolution or satellite overpass. In addition, environmental conditions like thick smoke plumes and dense vegetation cover significantly reduce fire detection. Ideally, the MODIS sensor routinely detects active fires of ~ 0.1 ha and, under ideal observational conditions, fires up to ~ 50 m^2 in size can be captured, but those of lesser extents or with low emitted fire radiative power (FRP) may not be detected [83]. Conversely, the VIIRS sensor has a minimum theoretical detectable fire size of ~ 20 m^2 at 1 200 K fires burning in the daytime and one half at 900 K instantaneous fires at night time [58].

 doi:10.20944/preprints202404.0307.v1

2.5. Intercomparison Analysis

In this section, we made an intercomparison between our validated BA product (hereinafter referred to as NEALGEBA; NE Algeria BA) and five existing BA products with different spatial resolutions and input sensor data in terms of omissions and commissions. We also conducted validation and performed temporal trends using the ground-based BA estimates from the DGF.

2.5.1. Spatial Accuracy

To highlight the differences in terms of burned patch delineation between NEALGEBA and existing BA products, we compared the accuracy metrics (CE, OE, DC, RelB) obtained for all the BA products. To this end, we used the same Sentinel-2 reference data at the same previously selected validation sites to validate the NEALGEBA map for 2017 to assess GABAM, C3SBA11, FireCCI51, MCD64A1 and EFFIS because this is the common year between all these BA products [45,46]. The 2017 BA maps from FireCCI51 and MCD64A1 were already available as image collections in the GEE's data catalogue, and were directly evaluated against S2RD in the assessment tool. The GABAM, C3SBA11 and EFFIS maps were firstly adjusted to the required format and uploaded to the assessment tool. It is important to note that GABAM does not provide the burn date, as required by the assessment tool, but indicates only the burn year. To overcome this situation, we assigned approximate burn detection dates to the burned patches on the 2017 GABAM map by overlaying the BA map from NEALGEBA. The burned patches with the largest overlap were assigned the same burn detection date, whereas those with no overlap were not dated.

2.5.2. Cross-Correlation with Ground-Based Fire Dataset

To assess NEALGEBA performance in BA estimation terms, we performed a cross-correlation analysis among the total annual BA estimates from our product, existing BA products and the ground-based fire dataset from the DGF over the 13 available years during the 2004–2019 period using the "PerformanceAnalytics" R-package [84]. However, the C3SBA11 product was not considered since only three years were available (2017, 2018, and 2019) among the overlapping years between the BA products. Here and in the subsequent step (Section 2.5.3), exclusively, the land cover class 10 (tree cover), class 20 (shrubland), and class 30 (grassland) from the ESA WorldCover map 2021 [52] were assumed to represent the spatial extent of natural vegetation landscapes and were used to mask out detected burned patches outside these classes from NEALGEBA and existing BA products. This was done following the definition of wildland fires in Algeria [50] based on which the fraction of cropland fires is not taken into consideration when reporting BA estimates by the local forest services of the DGF.

2.5.3. Temporal Burned Area Trends

We analyzed the temporal trends of the annual BA estimates from filtered NEALGEBA and the DGF datasets for the 1985–2023 period (the DGF dataset lacks data for 1984) using the Mann-Kendall trend test [85,86] and Sen's slope estimator [87]. These two non-parametric methods are widely used to test the significance of trends in fire regimes [88].

 doi:10.20944/preprints202404.0307.v1

3. Results

3.1. Analysis of the Generated BA Product

3.1.1. Spatial and Temporal Patterns

The BA mapping phase resulted in the generation of spatially explicit annual BA maps covering all fires occurring in the natural landscapes and rural areas of the six wilayas in the NE coast of Algeria at the 30-m resolution for the 1984–2023 period (Figure 4a). In the last four decades, the total mapped BA was 1.16 M ha with an average of 29,130.5 ha year^{-1} affecting forests (65.2%), shrublands (9.30%), grassland (22.2%), croplands (2.79%) and other types (< 0.6%). This BA is double the official BA estimate from the DGF (0.65 M ha). The total annual BA showed wide temporal variability in the last 40 years, with 68.8% of the total BA occurring in 13 peak years above the mean. The most extreme years were 1994, 2000, 2017 and 2021, when more than 15.0%, 6.6%, 5.3% and 8.4% of the total BA were respectively observed. These years accounted for up to 35.3% of the total BA in the entire time series. Conversely, the lowest annual BAs were found in 1984, 1996 and 2018, which represent less than 1% of the total BA over the entire study period (Figure 4b). The study area showed a high fire recurrence rate with more than 52.7% of the total BA affected by two fire events or more in the last four decades (Figure 4c). Indeed, the total mapped BA (1.16 M ha) was twice the extent of the land affected by at least one fire (0.58 M ha). Only 47.3% of this land was burned once, while 25.9% was burned twice and 25.8% was affected by three fires or more (Figure 4c).

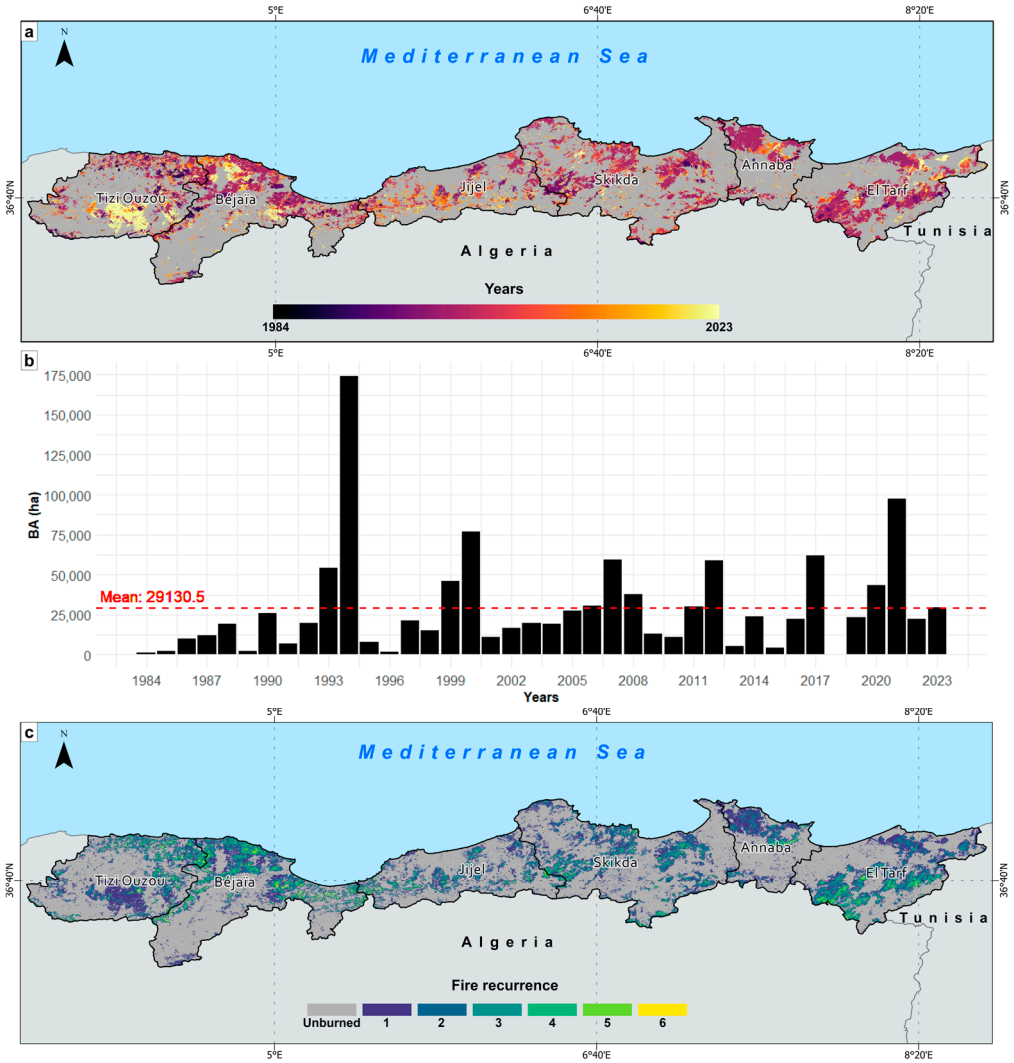

Figure 4. Spatio-temporal patterns of fires according to NEALGEBA in NE Algeria from 1984 to 2023. (**a**) Spatial extent of fires; (**b**) Temporal distribution of the total annual BA; (**c**) Fire recurrence.

Preprints.org (www.preprints.org) | NOT PEER-REVIEWED | Posted: 3 April 2024 doi:10.20944/preprints202404.0307.v1

Besides temporal variability, the annual BA showed wide spatial variability between the different wilayas. The fraction of burned burnable land represented 101.2% (2.53% year^{-1}) in El-Tarf, 94.5% (2.36% year^{-1}) in Béjaïa, 81% (2.025% year^{-1}) in Tizi Ouzou, 78.6% (1.96% year^{-1}) in Annaba, 67.3% (1.68% year^{-1}) in Skikda and 61.8% (1.54% year^{-1}) in Jijel. When looking at the fire event spatial pattern independently of their surface, the kernel density estimation (KDE) analysis showed fire hotspots in the Tizi Ouzou and Béjaïa wilayas, which are high ignition rates in these wilayas (Figure 5a). However, when fires were weighted by their sizes, the WKDE showed more fire hotspots in the Skikda, Annaba, and El-Tarf wilayas (Figure 5b).

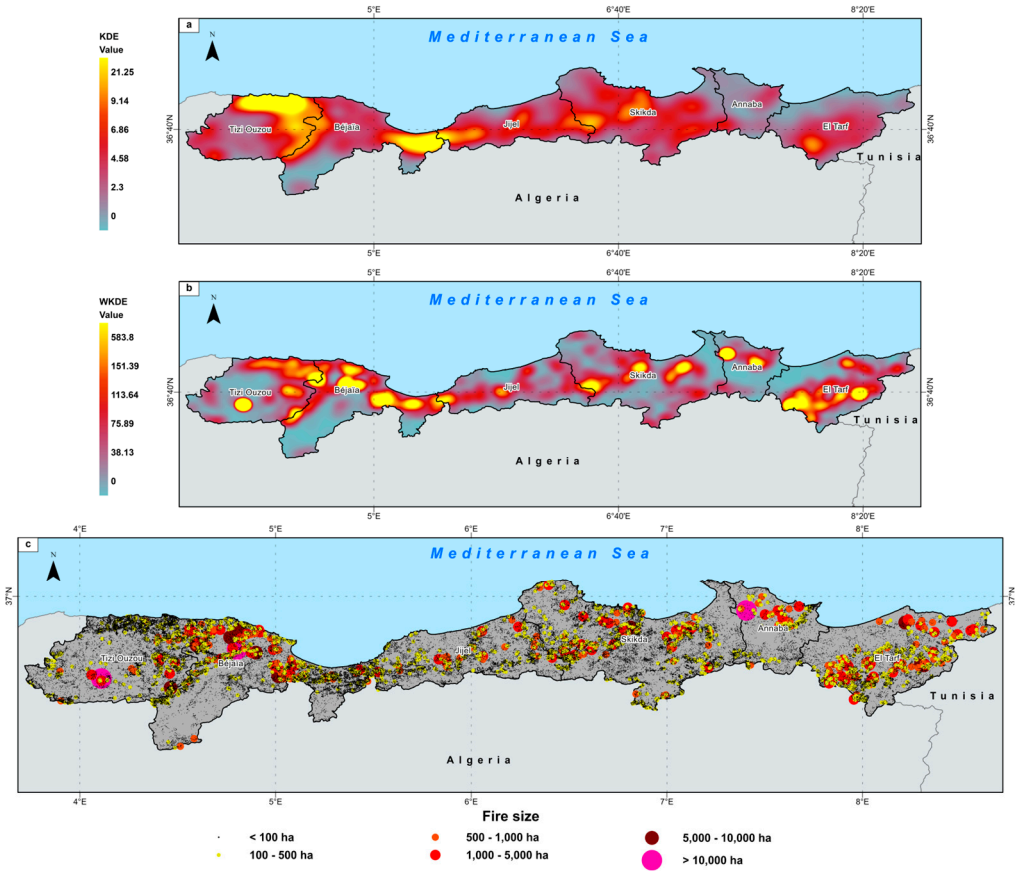

Figure 5. Kernel density distribution according to NEALGEBA in NE Algeria from 1984 to 2023. (**a**) Kernel density estimation (KDE); (**b**) BA-weighted kernel density estimation (WKDE); (**c**) Spatial distribution of fire size classes.

3.1.2. Fire-Size Distribution

The minimum detectable fire size equaled ~ 0.1 ha, which corresponded to the areal unit covered by a Landsat pixel on the ground. The maximum fire size was 26,300 ha, which occurred in the Tizi Ouzou wilaya in 2021. Fire size distribution using all the fire patches (n = 98,259) followed the self-organized criticality hypothesis [89] up to a fire size threshold of 1.5 ha, below which some small fires could be missing (Figure 6).

Preprints.org (www.preprints.org) | NOT PEER-REVIEWED | Posted: 3 April 2024 doi:10.20944/preprints202404.0307.v1

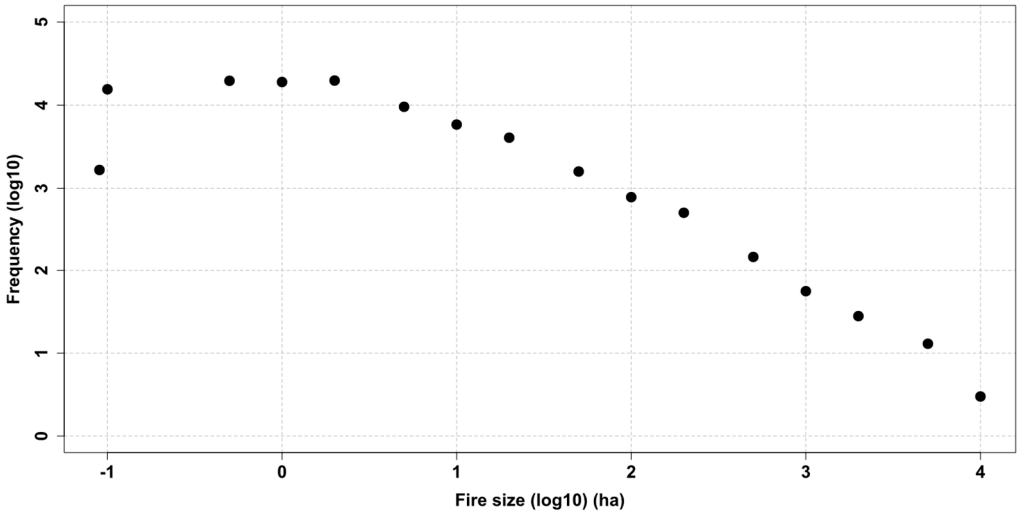

Figure 6. Fire size distribution: fire size (ha) and fire frequency on the log10 scale.

3.1.3. Fire Seasonality

Fire seasonality, based on fire number and BA, could be generated on 22,115 fire patches, which could be dated out of the 66,018 fire patches identified over the 2001–2023 period when the VIIRS/MODIS hotspots were available. NE Algeria displays typical Mediterranean fire activity, and July and August are the most burnable months, which prolong to September and October (Figure 7).

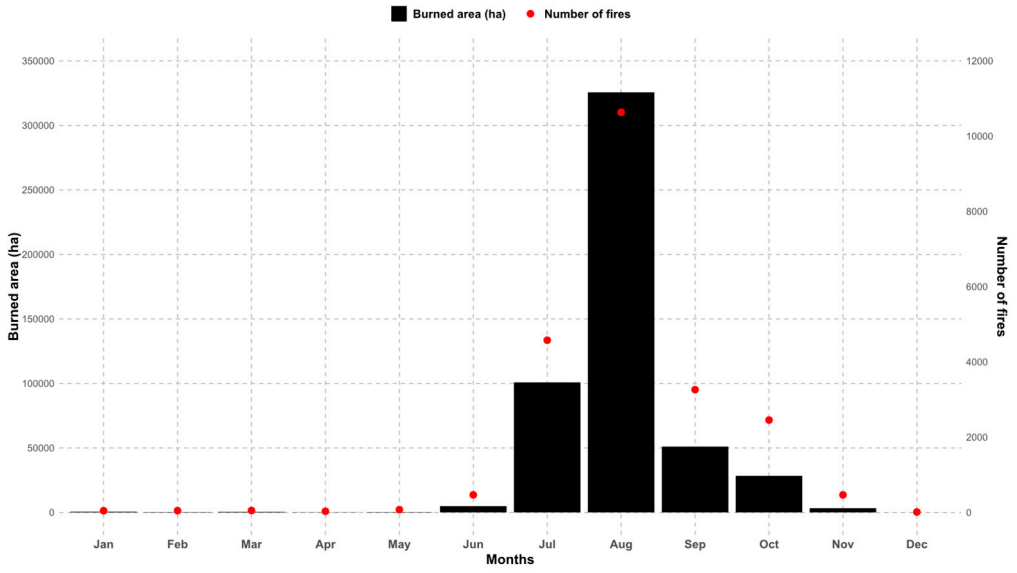

Figure 7. Fire seasonality based on monthly burned area and fire frequency during the 2001–2023 period.

3.2. Spatio-Temporal Validation

3.2.1. Spatial Validation

The results of the accuracy assessment of the NEALGEBA maps of 2017 and 2021 at the 10 validation sites using S2RD are presented in Table 2. The corresponding validation images are found in Figure B1 and Figure B2. For the validation year 2017, the OA was 98.22%, with a CE of 7.96%, an OE of 8.19% and a DC of 91.92%. Notably, validation site 31SEA-E3 had the highest OE with 30.16%,

 doi:10.20944/preprints202404.0307.v1

which resulted in an underestimation of the total BA of 23.19% and the lowest DC (79%) of all the validation sites. The highest commissions (CE = 9.65%) occurred at 32SMF-Y3. The overall RelB indicated a slight underestimation of the total BA of 0.24%. The total area correctly detected as burned was 195.51 km², while 1,700 km² of unburned surface was correctly detected at all the validation sites (covering 2,000 km²). Additionally, the product misclassified 16.92 km² of the unburned surface as burned and omitted 17.43 km² of the burned surfaces. For 2021, the product achieved similar results to those for 2017 in terms of OA (98.15%) and commissions (7.92%), albeit with a twofold decrease in omissions (4.76%) that resulted in a higher DC (93.63%). Of all the validation sites, the highest commissions and omissions were for 32SKF-P3 with values of 25.38% and 14.88%, respectively, and an RelB value of 14.08%. The DC was the lowest at all the validation sites with 79.52%. The total area correctly detected as burned was 270.70 km² and 1,689.84 km² was correctly detected as unburned. There were instances where the product incorrectly classified 25.53 km² of unburned surface as burned and omitted 13.52 km² of the burned surface. Overall, cloud coverage was the primary source of BA omissions, whereas most commissions were caused by the BA algorithm over land covers spectrally akin to the burned surfaces, such as harvested croplands, labored lands, water bodies and shadowed areas.

Table 2. Spatial validation results of the NEALGEBA maps of 2017 and 2021 at all the validation sites.

Sentinel-2 tiles	Validation sites	Accuracy metrics									
		Years	CE	OE	OA	DC	RelB	SurfBA	SurfUB	SurfCE	SurfOE
31SEA	E-3	2017	9.08	30.16	98.99	79.00	-23.19	8.46	430.61	0.84	3.65
	F-3	2021	9.71	2.92	96.91	93.56	7.52	99.57	333.54	11.06	2.99
31SFA	I-2	2017	6.06	4.93	98.81	94.50	1.21	23.43	202.19	1.51	1.21
	G-3	2021	4.65	4.93	97.40	95.21	-0.29	118.71	329.53	7.67	6.15
32SKF	Q-3	2017	7.36	12.13	98.11	90.19	-5.16	41.67	428.13	3.31	5.75
	P-3	2021	25.38	14.88	98.78	79.52	14.08	9.85	400.11	3.35	1.72
32SLF	V-2	2017	5.51	10.00	98.51	92.19	-4.75	36.50	372.80	2.13	4.06
	U-2	2021	11.56	6.37	99.53	90.96	5.87	6.79	277.59	0.89	0.46
32SMF	Y-3	2017	9.65	3.12	96.73	93.50	7.22	85.45	266.27	9.13	2.76
	X-3	2021	6.66	5.78	98.78	93.78	0.94	35.78	349.07	2.55	2.19
Overall		2017	7.96	8.19	98.22	91.92	-0.24	195.51	1 700.01	16.92	17.43
		2021	7.92	4.76	98.15	93.63	3.43	270.70	1 689.84	25.53	13.52

CE: Commission Error, OE: Omission Error, OA: Overall Accuracy, DC: Dice coefficient, and RelB: Relative Bias, all expressed as percentages. SurfBA: surface correctly detected as burned, SurfUB: surface correctly detected as unburned, SurfCE: committed burned surface, SurfOE: omitted burned surface, all expressed as km².

3.2.2. Temporal Validation

The NEALGEBA product showed significant fire detection delay compared to the active fire hotspots from MODIS and VIIRS. On average, burned pixels were detected 42.55 days after hotspot detection: 21.07% on the first 15 days, 46.47% in the first month and 75.67% in a 2-month window (Figure 8). This disparity was attributed mainly to Landsat's low temporal revisit frequency (8–16 days), which could be worsened by the unavailability of cloud-free images for BA extraction purposes.

Preprints.org (www.preprints.org) | NOT PEER-REVIEWED | Posted: 3 April 2024 doi:10.20944/preprints202404.0307.v1

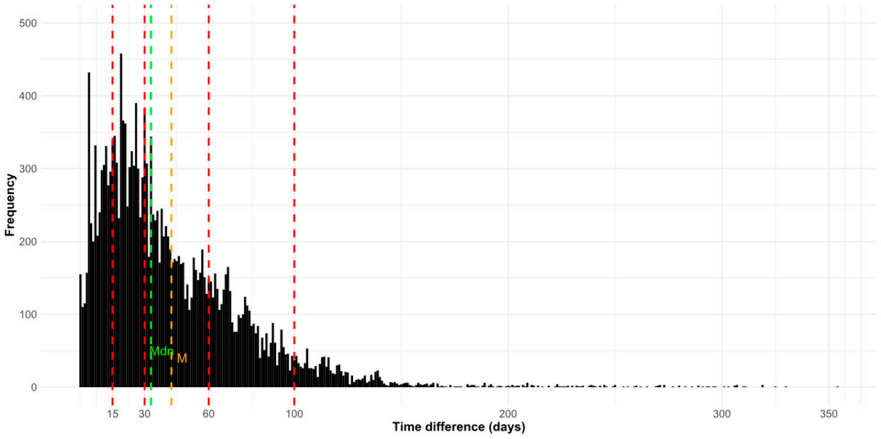

Figure 8. Distribution of the temporal difference in days between the burn detection dates from NEALGEBA and the active fire dates from MODIS and VIIRS across the study area from 2001 to 2023. M: Mean and Mdn: Median.

3.3. Intercomparison Analysis

3.3.1. Spatial Accuracy

The evaluation of the NEALGEBA product versus existing BA products showed our product's overall outperformance (Figure 9). Indeed, NEALGEBA had the lowest CE (7.96%), the highest DC (91.92%) and the best total BA estimation compared to S2RD (RelB = -0.24%). Despite being generated using the same input data (30 m Landsat images) and having a lower OE (3.89%), GABAM obtained a higher CE (13.33%) than NEALGEBA (7.96%), which resulted in an overestimated BA (RelB = 10.89%) compared to our product (RelB = -0.24%). As expected, coarser resolution products based on MODIS and Sentinel-3 OLCI: FireCCI51, MCD64A1, EFFIS and C3SBA11, produced the highest CEs and OEs, the lowest DCs with a significant lack of estimation of the total BA compared to S2RD. Specifically, FireCCI51, C3SBA11 and MCD64A1 had CEs ≥ 37.43%, which resulted in a marked overestimation of the total BA that reached 58.39%, 43.10 %, and 36.03%, respectively. However, these three products had relatively lower omissions ≤ 14.89%, compared to the EFFIS product (≥ 33.26%). The last one had the highest OE of all the assessed BA products, which led to the highest BA underestimation rate (RelB = -12.69%). Detailed results of the accuracy assessment of the GABAM, FireCCI51, C3SBA11, MCD64A1 and EFFIS BA maps of 2017, along with their corresponding validation images, appear in Tables B1 to B5, and in Figures B3 to B7, respectively.

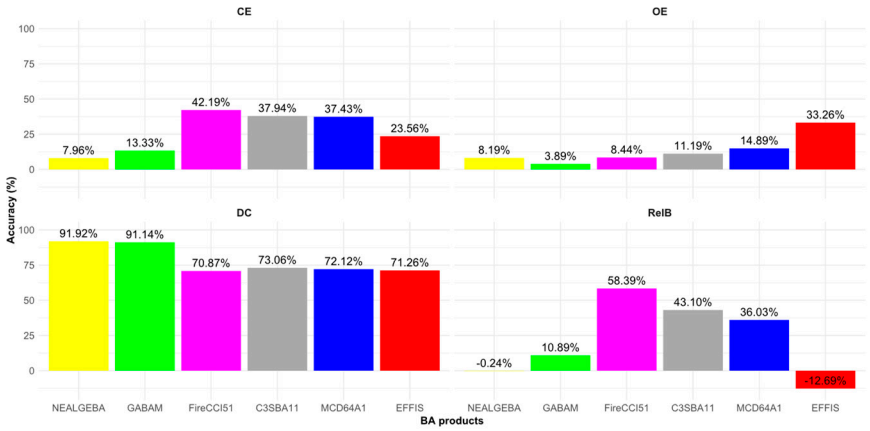

Figure 9. Accuracy metrics from the NEALGEBA, GABAM, FireCCI51, C3SBA11, MCD64A1 and EFFIS products. CE: Commission Error, OE: Omission Error, OA: Overall Accuracy, DC: Dice coefficient, and RelB: Relative Bias, all expressed as percentages.

Preprints.org (www.preprints.org) | NOT PEER-REVIEWED | Posted: 3 April 2024 doi:10.20944/preprints202404.0307.v1

The visual analysis clearly shows that all the detected large burned patches were consistent in all the BA products, although most relatively small fires were captured only by medium spatial resolution products (NEALGEBA and GABAM) (Figure 10a). GABAM demonstrated good spatial matching with S2RD, but obtained a high CE (13.33%) at all the validation sites (Table B1). This resulted in relatively extended burned patch limits compared to NEALGEBA. In other words, GABAM tended to overestimate the BA and included additional areas that may not have been burned. NEALGEBA showed higher OEs at all the validation sites, which resulted in slightly reduced burned patches compared to S2RD (Table 2). This indicates a tendency to exclude some burned patches, which leads to reduced BA compared to GABAM. These products tend to slightly underestimate or overestimate burned areas, respectively, compared to the higher resolution reference data from Sentinel-2. Furthermore, both omitted a few small burned patches and misclassified a few unburned pixels as burned. It is important to consider the trade-off between the CEs and OEs when evaluating the performance of BA maps.

Conversely, the larger pixel size in FireCCI51 (250 m), C3SBA11 (300 m), and MCD64A1 (500 m) led to size of burned patches being significantly overestimated. These products tended to overlook small fires and were unable to accurately delineate larger ones. They also displayed difficulty in discerning neighboring fire patches by perceiving them as single fire events, and they omitted the unburned islands in the main fire patches, which meant that the total BA was perpetually overestimated. EFFIS displayed a smoothing effect that oversimplified fire perimeters, with loss of details inside burned patches (unburned islands), which led to significant CEs. Particularly in this product, no fires were captured at validation site 31SEA-E3, an important part of the BA extent was omitted at validation site 32SKF-V2, and relatively small and spatially fragmented fires, at a distance from large burned patches, were completely omitted at the remaining validation sites. This resulted in significant OEs of the BA. As Figure 10b depicts, the total detected amount of BA at the five validation sites in S2RD of 2017 was 212.9 km². This was slightly reduced in NEALGEBA with 204.0 km² and slightly higher in GABAM with 231.4 km². Due to high commissions in FireCCI51, C3SBA11 and MCD64A1, the amount of BA was overestimated with 346.1 km², 316.1 km², and 296.9 km², respectively, whereas EFFIS significantly detected less BA with only 188.8 km² due to high omission values.

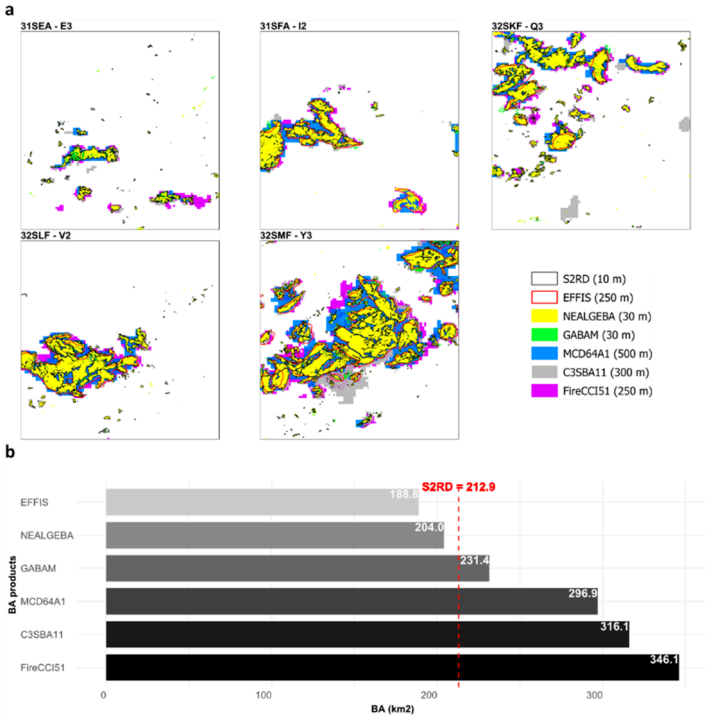

Figure 10. Burned area delineation (**a**) and total BA estimates (**b**) from NEALGEBA, GABAM, FireCCI51, C3SBA11, MCD64A1 and EFFIS, and the reference data (S2RD) at the validation sites in 2017.

 doi:10.20944/preprints202404.0307.v1

3.3.2. Cross-Correlation with Ground-Based Fire Dataset

The evaluation of the different BA products compared to the DGF dataset was done using the log10-transformed total annual BA estimates over the 13 overlapping years that comprised the 2004–2019 period between the different products. In general, the distinct BA products showed a strong correlation with the DGF data over the entire study area (Figure 11a). NEALGEBA, FireCCI51, and MCD64A1 obtained the highest correlations (r = 0.96), while GABAM yielded a slightly lower value (r = 0.94) even though it had the same spatial resolution as NEALGEBA (30 m). EFFIS had the lowest correlation with the DGF dataset. On the scale of the different wilayas, NEALGEBA demonstrated a better correspondence with the DGF estimates than existing BA products (Figure 11b).

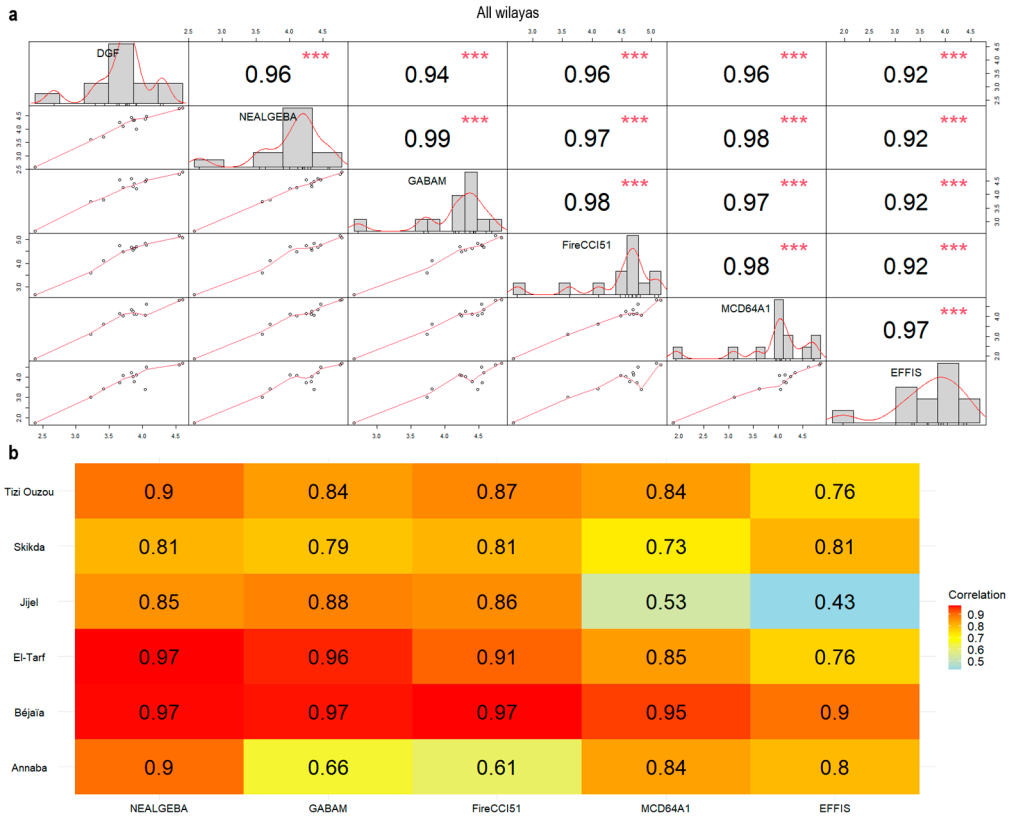

Figure 11. Pearson's correlation analysis of the total annual BA estimates from the BA products and the DGF dataset for all wilayas combined (**a**) and for each wilaya (**b**).

3.3.3. Temporal Trends of the Burned Area

Generally, the temporal evolution of total annual BA estimates from NEALGEBA and DGF displayed a consistent increasing trend over the 1985–2023 period (1984 is unavailable in the DGF dataset), yet differ in the annual rate, with NEALGEBA showing significant trends. For all the wilayas combined, NEALGEBA showed a significant increase rate of 532.4 ha year^{-1} at 10% (p-value = 0.053) in the total annual BA while DGF showed lower increase rate (197.1 ha year^{-1}; Figure 12a). At the wilaya scale, the annual BA from the two products showed significant positive trends at 5% (p-value ≤ 0.05) for the two products in Béjaïa and only significant for NEALGEBA in Jijel (p-value = 0.05) and in El-Tarf at 10% (p-value = 0.056). In general, NEALGEBA showed higher increased BA rates (182.2, 105.6 and 67.9 ha year^{-1} in Béjaïa, Jijel, Skikda and El-Tarf, respectively; Figure 12b).

 doi:10.20944/preprints202404.0307.v1

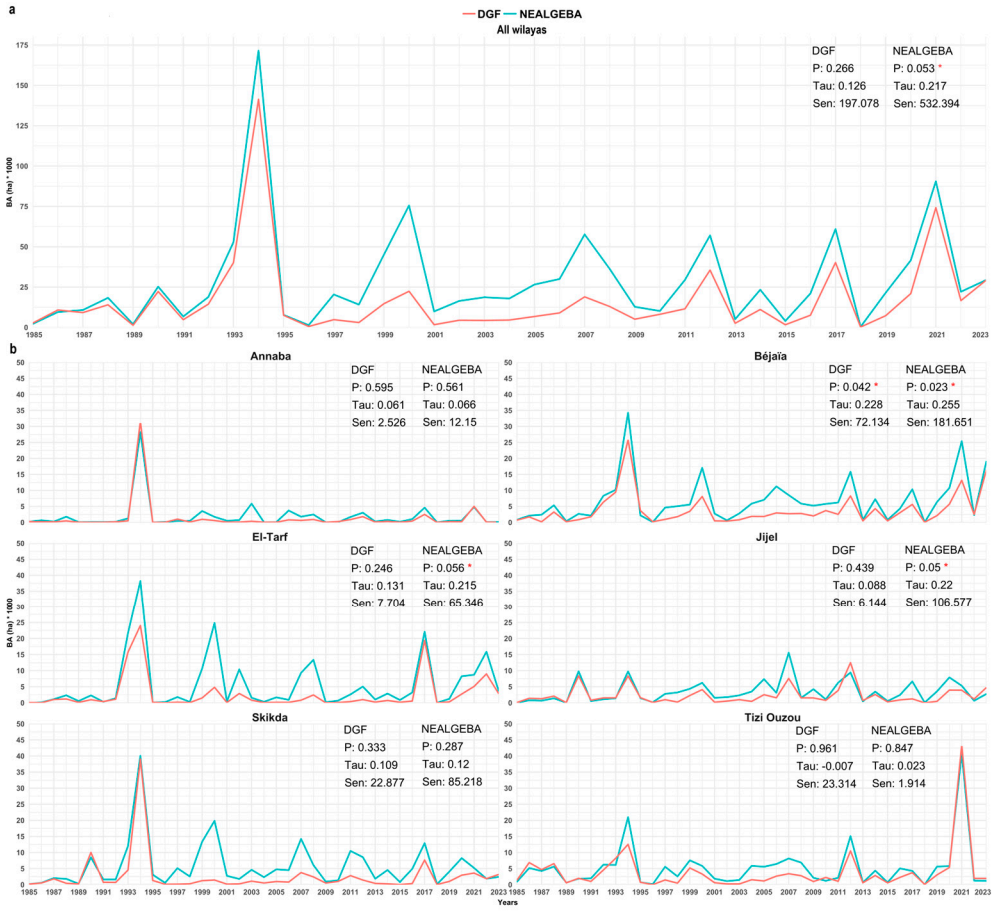

Figure 12. Temporal trends in the total annual BA estimates from NEALGEBA and DGF for the 1985–2023 period for all the wilayas combined (**a**) and for each wilaya (**b**). P: p-value, Tau: Kendall's Tau, Sen: Sen's slope. The red asterisk indicates statistically significant trends.

4. Discussion

In this analysis, we reconstructed and validated 40 years (1984–2023) of historical fire events at fine spatial resolution in typical Mediterranean ecosystems of NE Algeria. The newly generated NEALGEBA product represents the first and most extensive time series of BA in this part of the Mediterranean Basin, which faces a substantial fire occurrence threat. The BA product generation (phase I) proved the high potential and reliability of the BA Cartography tool in generating spatially consistent annual BA maps based on a Random Forest supervised classification and a two-phased strategy [42,62]. Despite being labor-intensive and heavily relying on the visual interpretation of pre- and postfire temporal composites, this semi-automatic procedure enabled high control over CEs and OEs and, thus, improved the BA product's quality. The analysts' expertise is more involved in selecting representative burned (seeds) and unburned samples with an iterative analysis of BA delineation [77], a considerable asset that is not provided with fully automated methods [32]. Additionally, the visual quality control and manual refinement of the generated fire perimeters allows to reduce potential anomalies such as those caused by the sensor. The RP, VA, VA dates, and the assessment tools, greatly facilitated the spatial validation exercise of satellite-derived BA products compared to previous studies [64,90], and all in accordance with the BA assessment standardized protocol endorsed by the CEOS. These tools ensured the creation of high-quality reference data (RP tool) from consecutive 10-m cloud-free Sentinel-2 images (VA Date) located at the validation sites preselected by stratified random sampling (VA tool). The assessment tool allowed a full-automatic comparison of the BA maps to the Sentinel-2 reference data, and reported accuracy metrics (CE, OE, DC and RelB) at each validation site.

 doi:10.20944/preprints202404.0307.v1

The accuracy assessment of the 2017 and 2021 NEALGEBA maps showed remarkable results with CEs of 7.96% and 7.92%, OEs of 8.19% and 4.76% and DCs of 98.22% and 98.15%, respectively. These metrics are consistent with better performance than those obtained in the original case study in south-eastern Australia, in which a BA product for the 2019 / 2020 fire season was generated and validated using the same input data with a CE of 11.80%, an OE of 8.90% and a DC of 89.60% [42]. However, the larger pixel size (30 m) in NEALGEBA led to a subtle alteration in the extent of the burned patches, which meant that their boundaries slightly extended outwardly compared to the reference perimeters from the 10-m Sentinel-2 independent reference data. We also observed that almost all the spatially isolated small burned patches were misclassified as burned, and mainly in 2021. This was due to the algorithm's limitation to discriminate small spectrally confusing surfaces with a similar spectral response to the burned surfaces. For the 2021 fire season, most of the BAs were in mountainous areas, which made it quite challenging to select representative and sufficient burned seed pixels to capture the entire burned patches, and thus, to reduce omissions. We attempted to avoid burned pixels in shadowed areas to reduce commissions on the classification map. We found that the algorithm failed to ensure the continuity of some large burned patches, and omissions occurred mostly on the edges of the main burned patches and on unburned islands with very few small isolated burned patches that were completely omitted. Overall, the obtained accuracy metrics indicated the NEALGEBA product's spatial consistency. However, the temporal validation using the active fire hotspots from MODIS and VIIRS underlined its limitation for accurately reporting fire events over time. This was explained by the long revisit time of the Landsat satellites (8–16 days), atmospheric conditions (i.e., clouds) and temporal compositing, which could significantly delay BA detection. This is not uncommon in medium-resolution products [42,46] compared to MODIS-derived products that incorporate active fire information [23,28], and underscores the need for further development to improve temporal uncertainty. Employing data from satellite sensors with a higher observation frequency, such as Sentinel-2 and the active fire hotspots from VIIRS, would reduce temporal reporting delays [26].

Coarse resolution BA products were found to significantly overestimate the total BA on a finer spatial scale due to a larger pixel size (≥ 250 m), unlike the continental scale on which the total BA was overly underestimated when compared to more accurate data from Sentinel-2 MSI sensor [26,27,36,37]. In addition, their limited temporal coverage (2001–present) prevents long-term fire studies compared to the BA products generated from the Landsat data archive dating back to 1984. The validation of the 2017 EFFIS BA map showed that the latter presented the highest omissions of all the assessed BA products, which resulted in a considerable underestimation of the total BA, plus a smoothing effect on fire perimeters that roughly delineated the burned patches. These inconsistencies have been previously reported in [40,91,92], and are attributed mainly to the 250-m coarse-resolution input data from MODIS used to generate the EFFIS product. On the other hand, GABAM is, to date, the only available global high-resolution BA product to provide BA mapping at finer spatial resolution to reliably detect smaller burned patches [32]. However, this product was generated in yearly composites by providing only the burn year without indicating the approximate burn detection date, which prevents a fire seasonal analysis. Moreover, while GABAM has the longest time span amongst global BA products (1985–2019), some years remain unavailable. In addition to the reported commissions over agricultural lands, significant systematic errors were observed when we examined the GABAM annual maps versus the corresponding Landsat post-fire image composites in a Long SWIR/NIR/Red color composition and NEALGEBA. The former represents BA commissions over water bodies, unburned forest areas, clouds, flares in oil/gas facilities and Landsat strip errors (Figure B8 a to c). Additionally, significant errors occurred in 2002 (Figure B8 d) and were perhaps caused by the significant alteration of the primary functioning mode of Landsat-5 TM's scan mirror, known as the scan angle monitor (SAM), which led to internal synchronization problems. This failure caused diagonal patches of anomalous observations with very high reflectance values in the long shortwave infrared (SWIR2) towards the scene footprint edges, and led to false fire detections. The SAM system was then switched to an alternative one called the bumper mode [93], which overcame this anomaly. The semi-automatic BA extraction procedure, which uses the BA

 doi:10.20944/preprints202404.0307.v1

Cartography tool along with a thorough visual inspection of the mapped burned patches, allowed these anomalies to be mitigated and consistent results to be obtained on the NEALGEBA annual maps. Overall, these limitations highlight the challenges and complexities involved in using existing BA products to accurately characterize local and regional fire regimes. The newly generated BA product herein presented serves as a surrogate to existing BA products by offering improved spatio-temporal resolutions allowing for a thorough assessment of fire impacts on forest ecosystems and, in turn, assists in designing strategies and adapted action plans to mitigate their severity in NE Algeria. Additionally, BAMTs can be easily leveraged by forests and protected areas managers in Algeria to operationally extract burned perimeters and to integrate complementary field data, especially the day and time of ignition, which reduces temporal uncertainties.

Our first evaluation of the newly generated NEALGEBA could properly address the fire seasonal distribution that spans from July to October and peaks in August. This result is in accordance with the seasonal drought and fire weather index seasonality characterizing our region [5]. Similar fire season length is reported in neighboring Tunisia [13] and in Portugal [94], and a slightly longer than the usual July-September fire season reported in Morocco [95], Italy [96,97], Greece [98], Bulgaria [99], and the Iberian Peninsula [100]. The length of the fire season in our region may be shaped by the early and late fire-prone weather conditions favored by climate change effects and socio-economic factors [5,9]. Regarding affected vegetation, we obtained a fraction of burnable areas affected by fires reaching 2.95% year^{-1} in fair agreement with Portugal (3.31%), making our BA estimates on the highest range of variability observed in the Mediterranean Basin. Only 0.19% was observed from Tunisia [13], Lebanon (0.58%), France (0.53%), Greece (0.57%), Spain (0.84%) and Italy (1.14%), as reviewed in [10]. We also detected an increasing trend in BA (532.4 ha year^{-1}) over the region. This trend is different from that in the northern part of the Mediterranean, where a general decreasing fire trend has been observed [101]. More precisely, an abrupt decrease has been observed in France in 1990 with increasing firefighting expenditures [60], and an increase in the 1980s and 1990s then a decrease since 2000 in Spain owing to land abandonment [59,102], and a decreasing trend was observed in Greece [14]. In the middle east and north Africa, no trends have been particularly observed since the 1980s [10,13], consistent with our study. However, the recent collapse of political regimes that have led to an abrupt increase in the BA in Tunisia [103], that we did not detect in Algeria not affected by this political collapse. Throughout history, Algeria has although been marked by significant political events that have led to heavy burning period, such as the Algerian Civil War (the Black Decade) in the 1990s [6], which was reflected by the highest peak in BA observed in 1994. Algeria has remained quite stable since 2011, when the Arab Spring started in the southern Mediterranean Basin and did not, thus, affect the BA during this recent period. Here we note the exceptional heat wave that hit the region in 2023 with record-breaking temperatures in April [104] and in July 2023, and with some casualties during fire events, which were widely reported in the media, but did not lead to the most extreme fire year compared to 1994 and 2021. Hence, NEALGEBA appears as a keystone database to provide accurate information on burned area and its temporal trends, and as a reference database to allow for the objective contextualization of fire years, to be further used in fire weather analyses, fire impacts assessments, fire model benchmarking or euro-Mediterranean initiatives of fire-related issues.

In its current version, NEALGEBA covers all types of fires that have occurred across all landscapes in NE Algeria from 1984 through 2023. However, this product, as the case with all satellite-derived BA products, exhibits specific limitations that necessitate reporting for future improvements. First, the burn dates indicated in our product do not match the effective fire dates, when the fires were actively burning. In fact, the BA Cartography tool computes the modal date from all pixels within each detected burned patch in the yearly Landsat post-fire composite. This results in significant fire detection delay, which impacts the product's temporal fire reporting accuracy, especially in large fires lasting several days. We highlight here that using data at a higher temporal resolution from Sentinel-2 MSI could significantly reduce this disparity [26,27,43]. Second, the product's commission errors were primarily observed over agricultural lands (harvested or ploughed croplands) which exhibit similar spectral features as to that of burned areas, characterized by abrupt

 doi:10.20944/preprints202404.0307.v1

changes in the reflectance data particularly in the near and shortwave infrared bands [27,32,35,61,62,105]. Here, we should also emphasize the high uncertainties associated with the detection of cropland fires [106]. Third, very large fire events enduring several days may not be effectively captured as single burned patches due to the low revisit frequency of Landsat satellites and availability of cloud-free image. Some large fire patches may not be spatially contiguous owing to low burn signal over shadowed areas, sparse vegetation, or discontinuity in vegetation cover. Additionally, spotting fires can result in spatially isolated burned islands from the main fire patches. Fourth, Landsat sensor anomalies were one of the main challenges especially the Landsat-7 ETM$^+$ SLC failure, which affected most of its time coverage. Post-processing procedures have been applied to mitigate commissions caused by these anomalies. However, some omissions or late fire detections (strips within an actual fire patch) should be acknowledged. Regarding future work, it is envisaged to complement the NEALGEBA product with detailed information contained in the ground-based fire inventories from local forest services of the DGF, especially for extreme fire events. For instance, burn detection dates can be corrected, thus reducing the product's temporal uncertainties. Possible attributes include: forest name or locality, date and exact time of ignition/intervention/extinction, burned vegetation type and species, land ownership, cause of ignition, perpetrator of the fire, fire reporter, weather conditions, participating bodies in fire suppression, damage assessment, and investigation. Ongoing efforts involve expanding NEALGEBA to a country-level BA product with continuous mapping of fire affected areas for the upcoming years using higher resolution imagery data from Sentinel-2 MSI. This aims to provide accurate characterization of the spatio-temporal patterns of fires across a larger geographical scale.

5. Conclusions

This paper presents a new spatially explicit fire database (NEALGEBA) in Mediterranean-type ecosystems of NE Algeria. This database is a reconstruction of 40 years (1984–2023) of historical fire patterns from Landsat data. NEALGEBA product offers the Algerian forest managers and policymakers valuable insights into the spatio-temporal distribution and magnitude of fires in this region which is prevalently and substantially vulnerable to extreme and large fires. Its provision of accurate and long-term BA mapping surpasses the limitations of existing global and regional BA product and is, thus, adequate for disentangling fire regime and identifying the key driving factors of fire occurrence and propagation in this part of the Mediterranean Basin. Furthermore, this dataset significantly contributes to further national and international fire hazard and impact assessments, and acts as a reference for contextualizing future weather extremes, such as the 2023 exceptional heat wave, which we show not to have led to the most extreme fire year over the last 40 years.

Author Contributions: Conceptualization, M.E.K., M.J.B. and H.M.; methodology, M.E.K., M.J.B. and H.M.; validation, M.E.K. and H.M.; formal analysis, M.E.K., A.K., A.M., F.M., M.J.B. and H.M.; investigation, M.E.K.; data curation, M.E.K.; writing—original draft preparation, M.E.K..; writing—review and editing, M.E.K., A.K., A.M., S.R., F.M., M.J.B. and H.M.; visualization, M.E.K. and H.M.; supervision, M.J.B. and H.M. All authors have read and agreed to the published version of the manuscript. This work is part of the PhD thesis of M.E.K.

Funding: This research received no external funding.

Institutional Review Board Statement: Not applicable.

Data Availability Statement: The NEALGEBA product is publicly available in Zenodo at https://doi.org/10.5281/zenodo.10684711 [107].

Acknowledgments: We thank Directorate General of Forests (DGF), Algeria for providing the national fire database. M.E.K. acknowledges the financial support granted by the Vice-Rectorate for International Relations and Cooperation for Development of the University of Alicante.

Conflicts of Interest: The authors declare no conflicts of interest.

 doi:10.20944/preprints202404.0307.v1

Appendix A

Table A1. Validation sites, validation periods and number of Sentinel-2 images for validation years 2017 and 2021.

Sentinel-2 tiles	Validation sites	Years	Validation period			
			Length in days	Start	End	Sentinel-2 images
31SEA	E-3	2017	170	19/06/2017	06/12/2017	20
	F-3	2021	120	23/06/2021	21/10/2021	20
31SFA	I-2	2017	170	19/06/2017	06/12/2017	18
	G-3	2021	225	11/05/2021	22/12/2021	29
32SKF	Q-3	2017	205	17/05/2017	08/12/2017	21
	P-3	2021	225	11/05/2021	22/12/2021	26
32SLF	V-2	2017	205	17/05/2017	08/12/2017	21
	U-2	2021	110	18/07/2021	05/11/2021	22
32SMF	Y-3	2017	185	04/05/2017	05/11/2017	21
	X-3	2021	230	08/05/2021	24/12/2021	29
Total Sentinel-2 images						227

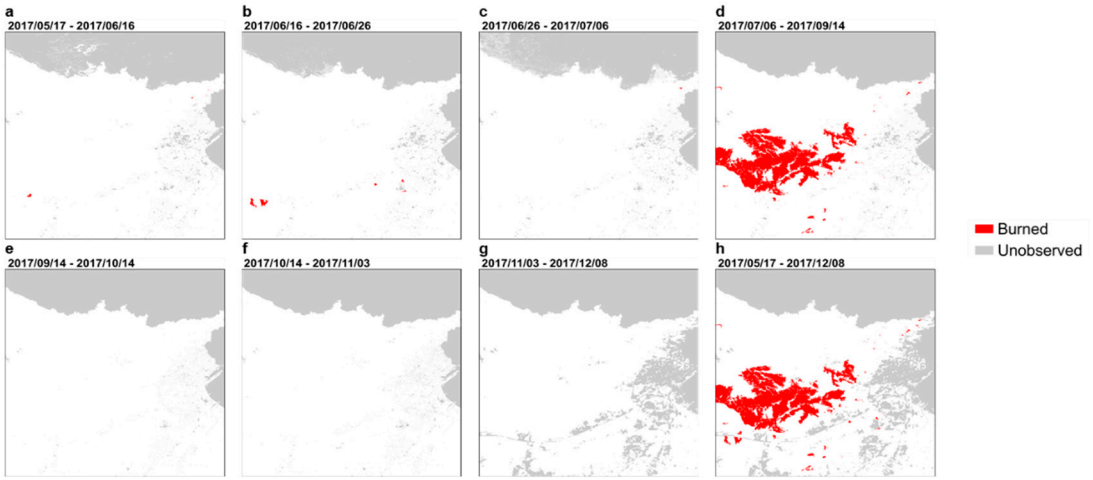

Figure A1. (a-g) Short units and (h) Long unit of the reference data at validation site 32SLF-V2 for the 2017 validation year.

Preprints.org (www.preprints.org) | NOT PEER-REVIEWED | Posted: 3 April 2024 doi:10.20944/preprints202404.0307.v1

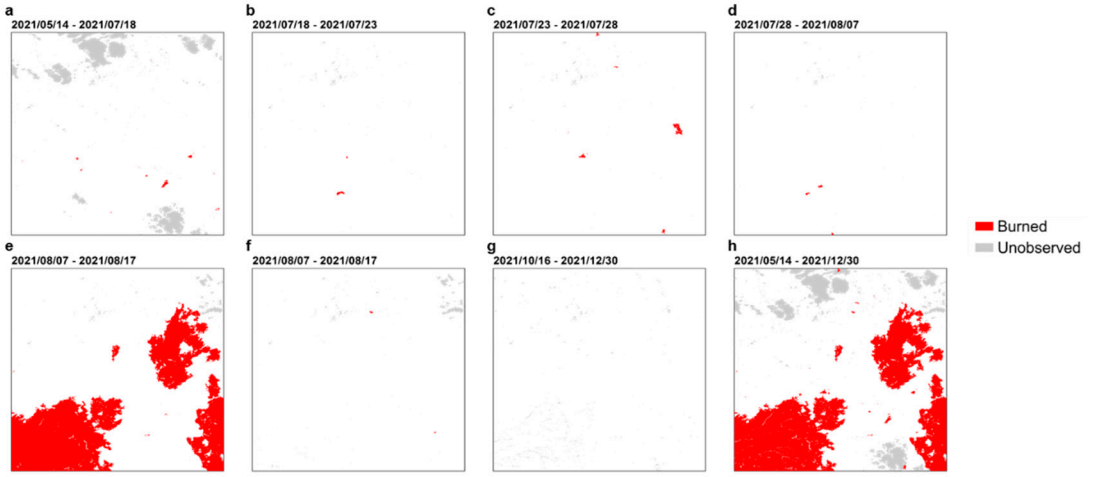

Figure A2. (a-g) Short units and (h) Long unit of the reference data at validation site 31SFA-G3 for the 2021 validation year.

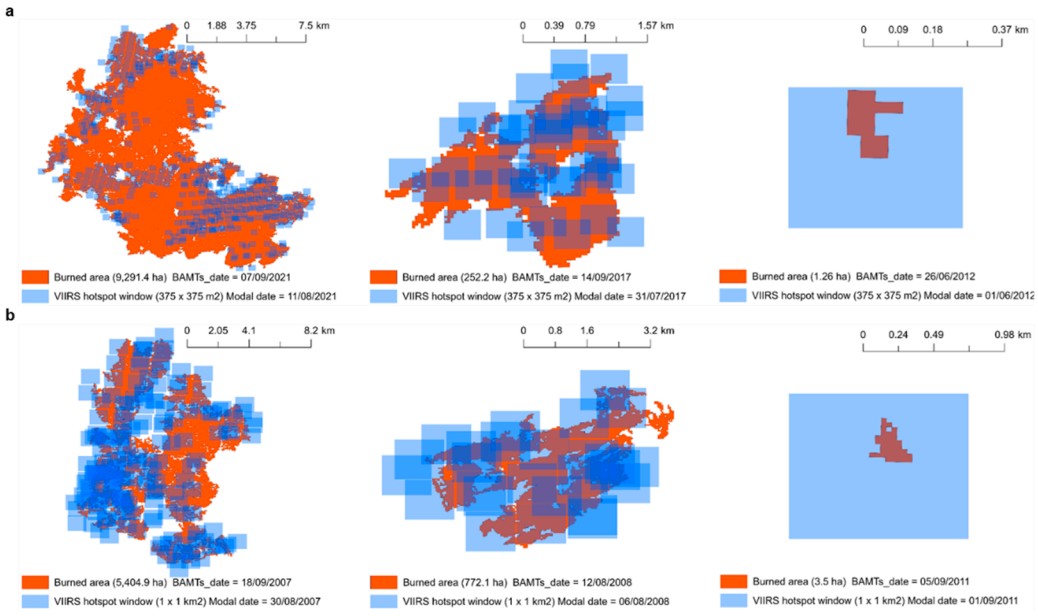

Figure A3. Comparison of the burn dates from BAMTs-derived product and hotspot windows from VIIRS (a) and MODIS (b).

Appendix B

Table B1. Spatial validation results of the 2017 GABAM map.

Sentinel-2 tile	Validation site	Accuracy metrics								
		CE	OE	OA	DC	RelB	SurfBA	SurfUB	SurfCE	SurfOE
31SEA	E-3	15.24	11.26	99.26	86.71	4.69	10.75	429.52	1.93	1.36
31SFA	I-2	10.88	1.99	98.49	93.35	9.97	24.15	200.76	2.95	0.49
32SKF	Q-3	14.60	4.50	97.94	90.16	11.83	45.29	423.70	7.75	2.14

 doi:10.20944/preprints202404.0307.v1

32SLF	V-2	7.29	7.75	98.54	92.48	-0.50	37.42	371.99	2.94	3.14
32SMF	Y-3	15.45	1.32	95.31	91.07	16.72	87.05	259.49	15.91	1.16
Overall		**13.33**	**3.89**	**97.94**	**91.14**	**10.89**	**204.65**	**1 685.45**	**31.47**	**8.29**

Table B2. Spatial validation results of the 2017 FireCCI51 map.

Sentinel-2 tile	Validation site	Accuracy metrics								
		CE	OE	OA	DC	RelB	SurfBA	SurfUB	SurfCE	SurfOE
31SEA	E-3	55.69	15.09	96.67	58.24	91.61	10.29	418.53	12.93	1.83
31SFA	I-2	33.22	4.87	94.37	78.47	42.46	23.44	192.04	11.66	1.20
32SKF	Q-3	40.82	20.10	92.55	68.00	35.02	37.90	405.31	26.14	9.53
32SLF	V-2	35.97	7.50	94.20	75.68	44.47	37.52	353.85	21.08	3.04
32SMF	Y-3	45.09	2.68	79.96	70.21	77.24	85.84	204.90	70.49	2.36
Overall		**42.19**	**8.44**	**91.70**	**70.87**	**58.39**	**194.98**	**1 574.63**	**142.30**	**17.96**

Table B3. Spatial validation results of the 2017 C3SBA11 map.

Sentinel-2 tile	Validation site	Accuracy metrics								
		CE	OE	OA	DC	RelB	SurfBA	SurfUB	SurfCE	SurfOE
31SEA	E-3	44.82	22.43	97.67	64.48	40.59	9.40	423.82	7.63	2.72
31SFA	I-2	30.97	6.42	94.78	79.45	35.55	23.06	193.36	10.34	1.58
32SKF	Q-3	39.27	27.29	92.64	66.18	19.74	34.48	409.14	22.30	12.94
32SLF	V-2	26.31	8.97	95.95	81.44	23.53	36.92	361.75	13.18	3.64
32SMF	Y-3	42.16	3.35	82.10	72.37	67.11	85.25	213.25	62.15	2.95
Overall		**37.94**	**11.19**	**92.77**	**73.06**	**43.10**	**189.11**	**1 601.32**	**115.61**	**23.83**

Table B4. Spatial validation results of the 2017 MCD64A1 map.

Sentinel-2 tile	Validation site	Accuracy metrics								
		CE	OE	OA	DC	RelB	SurfBA	SurfUB	SurfCE	SurfOE
31SEA	E-3	44.14	34.32	97.65	60.37	17.59	7.96	425.17	6.29	4.16
31SFA	I-2	35.10	9.65	93.69	75.54	39.21	22.26	191.66	12.04	2.38

 doi:10.20944/preprints202404.0307.v1

32SKF	Q-3	35.90	23.46	93.43	69.77	19.42	36.30	411.11	20.33	11.12
32SLF	V-2	33.42	11.79	94.53	75.88	32.50	35.78	356.97	17.96	4.78
32SMF	Y-3	39.62	10.50	83.21	72.11	48.23	78.94	223.59	51.80	9.26
Overall		**37.43**	**14.89**	**92.74**	**72.12**	**36.03**	**181.24**	**1 608.50**	**108.42**	**31.70**

Table B5. Spatial validation results of the 2017 EFFIS map.

Sentinel-2 tile	Validation site	Accuracy metrics								
		CE	OE	OA	DC	RelB	SurfBA	SurfUB	SurfCE	SurfOE
31SEA	E-3	0.00	100.00	97.27	0.00	-100.00	0.00	431.46	0.00	12.11
31SFA	I-2	18.12	15.98	96.27	82.93	2.61	20.70	199.12	4.58	3.94
32SKF	Q-3	24.45	63.64	92.53	49.09	-51.88	17.24	425.86	5.58	30.18
32SLF	V-2	21.77	21.94	95.74	78.14	-0.21	31.66	366.12	8.81	8.90
32SMF	Y-3	25.51	17.79	88.86	78.16	10.36	72.52	250.56	24.83	15.69
Overall		**23.56**	**33.26**	**94.06**	**71.26**	**-12.69**	**142.12**	**1 673.12**	**43.80**	**70.82**

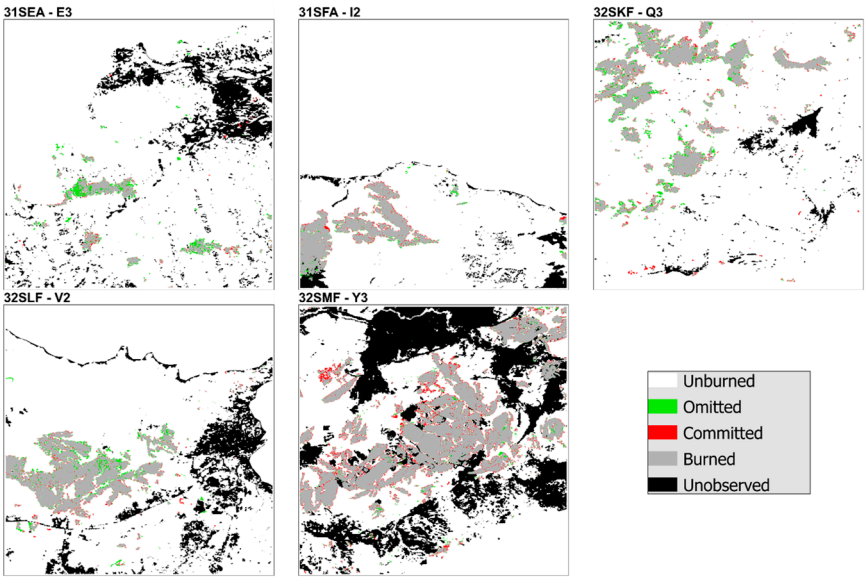

Figure B1. Correctly classified BA, commission and omission errors, and unobserved areas at the validation sites of 2017 for NEALGEBA.

 doi:10.20944/preprints202404.0307.v1

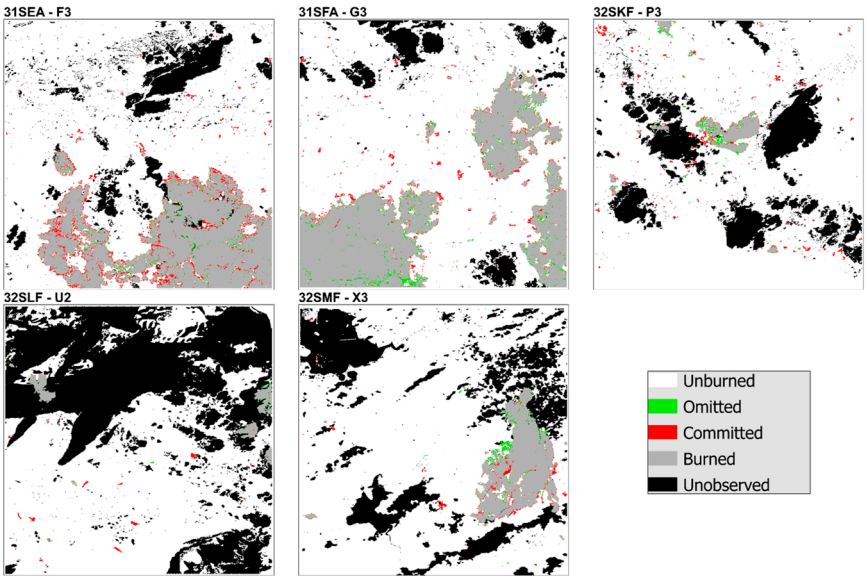

Figure B2. Correctly classified BA, commission and omission errors, and unobserved areas at the validation sites of 2021 for NEALGEBA.

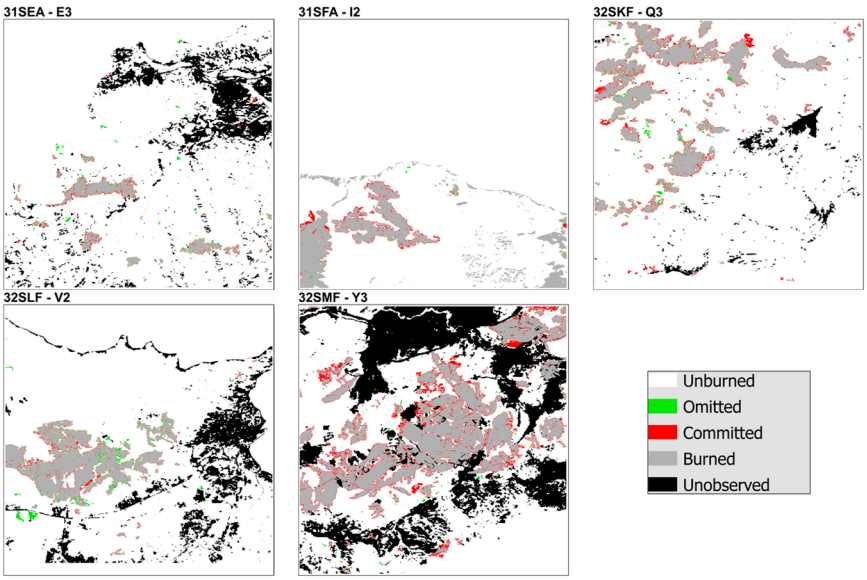

Figure B3. Correctly classified BA, commission and omission errors, and unobserved areas at the validation sites of 2017 for GABAM.

 doi:10.20944/preprints202404.0307.v1

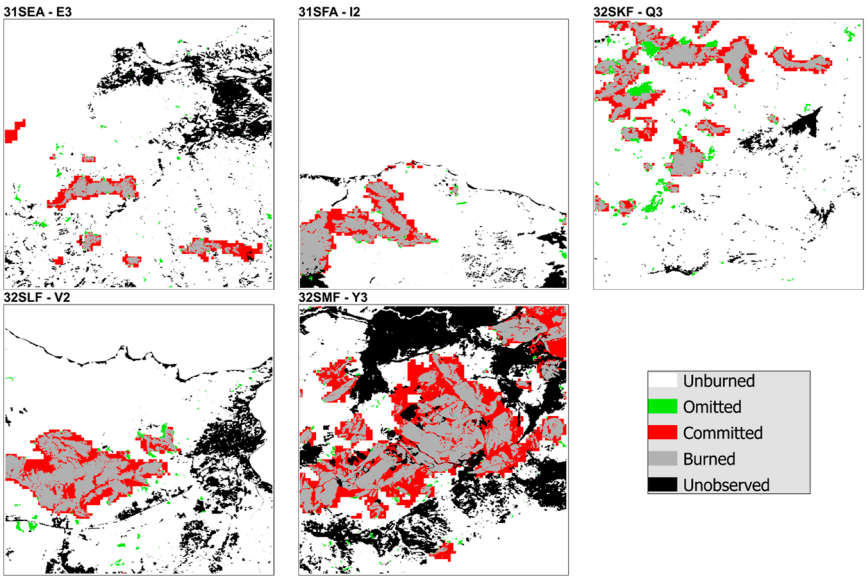

Figure B4. Correctly classified BA, commission and omission errors, and unobserved areas in the validation sites of 2017 for FireCCI51.

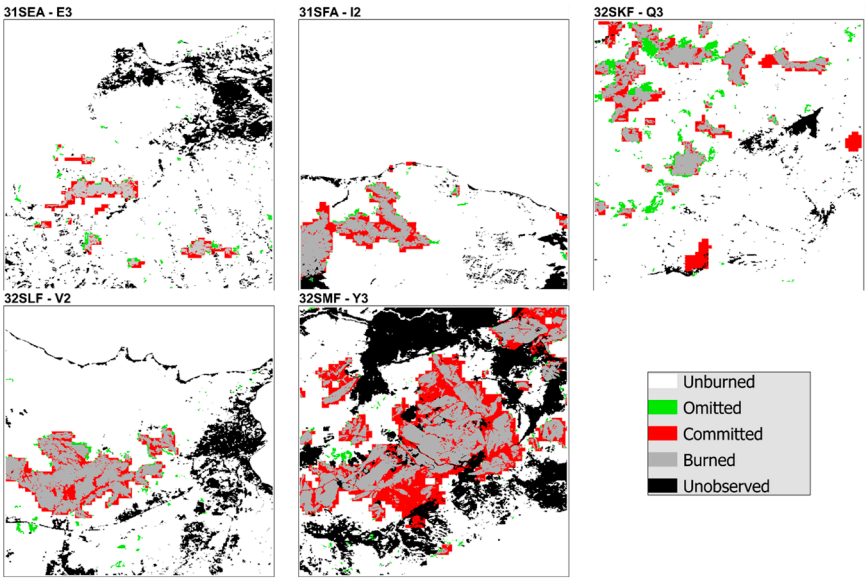

Figure B5. Correctly classified BA, commission and omission errors, and unobserved areas in the validation sites of 2017 for C3SBA11.

Preprints.org (www.preprints.org) | NOT PEER-REVIEWED | Posted: 3 April 2024 doi:10.20944/preprints202404.0307.v1

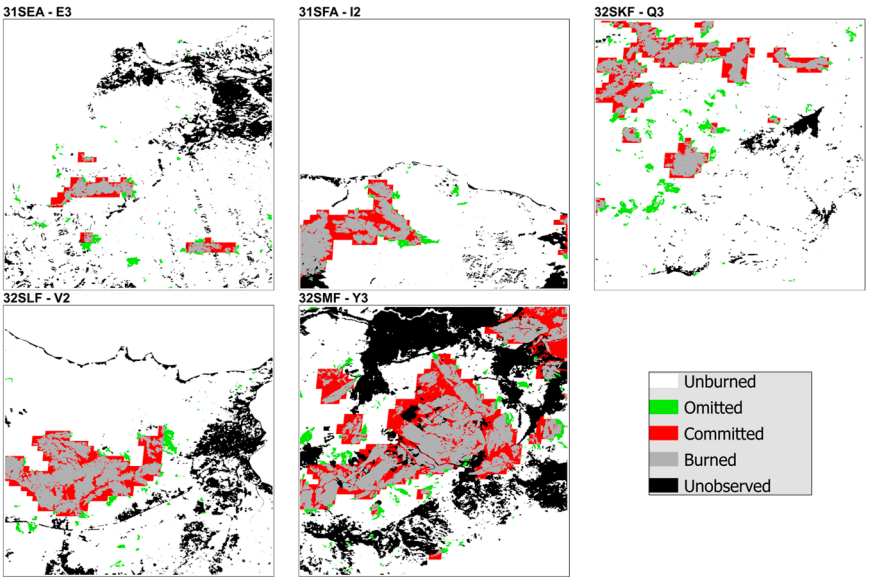

Figure B6. Correctly classified BA, commission and omission errors, and unobserved areas at the validation sites of 2017 for MCD64A1.

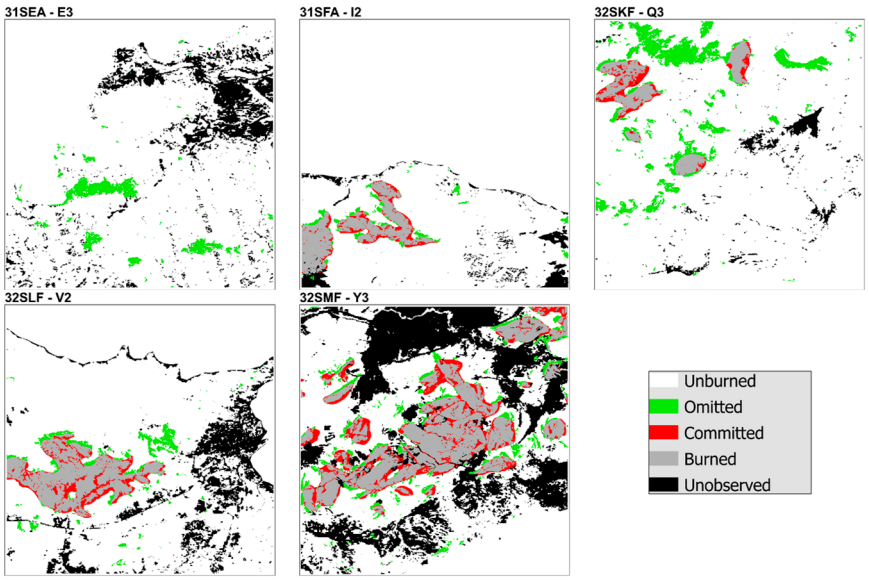

Figure B7. Correctly classified BA, commission and omission errors, and unobserved areas at the validation sites of 2017 for EFFIS.

 doi:10.20944/preprints202404.0307.v1

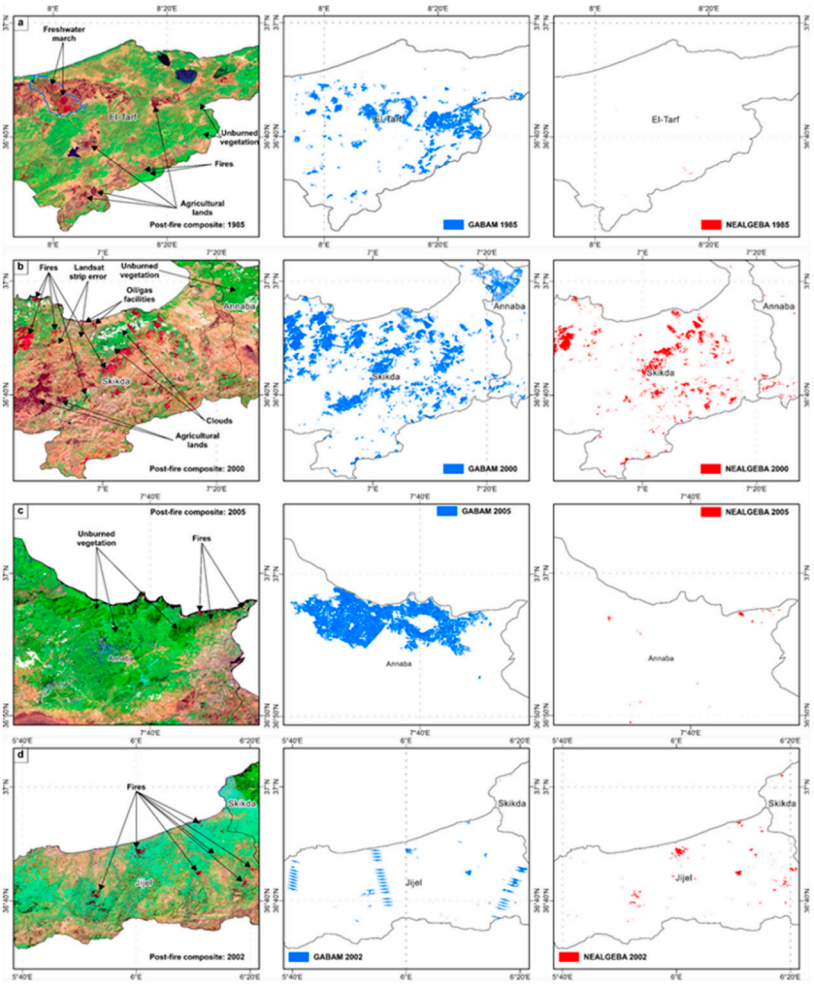

Figure B8. Examples of the BA detection anomalies observed on the GABAM annual BA maps (blue) vs. the corresponding post-fire image composites (displayed in a Long SWIR/NIR/Red colour composition) and NEALGEBA (red).

References

1. Bowman, D.M.J.S.; Balch, J.K.; Artaxo, P.; Bond, W.J.; Carlson, J.M.; Cochrane, M.A.; D'Antonio, C.M.; DeFries, R.S.; Doyle, J.C.; Harrison, S.P.; et al. Fire in the Earth System. Science (1979) 2009, 324.
2. Wu, C.; Venevsky, S.; Sitch, S.; Mercado, L.M.; Huntingford, C.; Staver, A.C. Historical and Future Global Burned Area with Changing Climate and Human Demography. One Earth 2021, 4, doi:10.1016/j.oneear.2021.03.002.
3. Seidl, R.; Schelhaas, M.J.; Rammer, W.; Verkerk, P.J. Increasing Forest Disturbances in Europe and Their Impact on Carbon Storage. Nat Clim Chang 2014, 4, doi:10.1038/nclimate2318.
4. Ruffault, J.; Curt, T.; Moron, V.; Trigo, R.M.; Mouillot, F.; Koutsias, N.; Pimont, F.; Martin-StPaul, N.; Barbero, R.; Dupuy, J.L.; et al. Increased Likelihood of Heat-Induced Large Wildfires in the Mediterranean Basin. Sci Rep 2020, 10, doi:10.1038/s41598-020-70069-z.
5. Curt, T.; Aini, A.; Dupire, S. Fire Activity in Mediterranean Forests (The Algerian Case). Fire 2020, 3, 1–17, doi:10.3390/fire3040058.
6. Madoui, A. Les Incendies de Forêt En Algérie. Historique, Bilan et Analyse. Forêt méditerranéenne 2002, 23, 23–30.
7. Sahar, O.; Leone, V.; Limani, H.; Rabia, N.; Meddour, R. Wildfire Risk and Its Perception in Kabylia (Algeria). IForest 2018, 11, doi:10.3832/ifor2546-011.
8. World Bank Note Sur Les Forêts Algériennes: Gestion Durable Des Forêts Pour Lutter Contre Les Feux de Forêts; Washington, DC: World Bank, 2023;
9. Meddour-Sahar, O. Wildfires in Algeria: Problems and Challenges. IForest 2015, 8, doi:10.3832/ifor1279-007.

10. Majdalani, G.; Koutsias, N.; Faour, G.; Adjizian-Gerard, J.; Mouillot, F. Fire Regime Analysis in Lebanon (2001–2020): Combining Remote Sensing Data in a Scarcely Documented Area. Fire 2022, 5, 141, doi:10.3390/fire5050141.
11. Chuvieco, E.; Aguado, I.; Salas, J.; García, M.; Yebra, M.; Oliva, P. Satellite Remote Sensing Contributions to Wildland Fire Science and Management. Current Forestry Reports 2020, 6.
12. Pereira, M.G.; Malamud, B.D.; Trigo, R.M.; Alves, P.I. The History and Characteristics of the 1980–2005 Portuguese Rural Fire Database. Natural Hazards and Earth System Sciences 2011, 11, 3343–3358, doi:https://doi.org/10.5194/nhess-11-3343-2011.
13. Belhadj-Khedher, C.; Koutsias, N.; Karamitsou, A.; Ei-Melki, T.; Ouelhazi, B.; Hamdi, A.; Nouri, H.; Mouillot, F. A Revised Historical Fire Regime Analysis in Tunisia (1985–2010) from a Critical Analysis of the National Fire Database and Remote Sensing. Forests 2018, 9, doi:10.3390/f9020059.
14. Koutsias, N.; Xanthopoulos, G.; Founda, D.; Xystrakis, F.; Nioti, F.; Pleniou, M.; Mallinis, G.; Arianoutsou, M. On the Relationships between Forest Fires and Weather Conditions in Greece from Long-Term National Observations (1894-2010). Int J Wildland Fire 2013, 22, doi:10.1071/WF12003.
15. Chuvieco, E.; Mouillot, F.; van der Werf, G.R.; San Miguel, J.; Tanasse, M.; Koutsias, N.; García, M.; Yebra, M.; Padilla, M.; Gitas, I.; et al. Historical Background and Current Developments for Mapping Burned Area from Satellite Earth Observation. Remote Sens Environ 2019, 225, doi:10.1016/j.rse.2019.02.013.
16. Andela, N.; Morton, D.C.; Giglio, L.; Chen, Y.; van der Werf, G.R.; Kasibhatla, P.S.; DeFries, R.S.; Collatz, G.J.; Hantson, S.; Kloster, S. A Human-Driven Decline in Global Burned Area. Science (1979) 2017, 356, 1356–1362, doi:https://doi.org/10.1126/science.aal4108.
17. García, M.; Pettinari, M.L.; Chuvieco, E.; Salas, J.; Mouillot, F.; Chen, W.; Aguado, I. Characterizing Global Fire Regimes from Satellite-Derived Products. Forests 2022, 13, 699, doi:https://doi.org/10.3390/f13050699.
18. Archibald, S.; Lehmann, C.E.R.; Gómez-Dans, J.L.; Bradstock, R.A. Defining Pyromes and Global Syndromes of Fire Regimes. Proc Natl Acad Sci U S A 2013, 110, doi:10.1073/pnas.1211466110.
19. Shi, K.; Touge, Y. Characterization of Global Wildfire Burned Area Spatiotemporal Patterns and Underlying Climatic Causes. Sci Rep 2022, 12, doi:10.1038/s41598-021-04726-2.
20. Van Wees, D.; Van Der Werf, G.R. Modelling Biomass Burning Emissions and the Effect of Spatial Resolution: A Case Study for Africa Based on the Global Fire Emissions Database (GFED). Geosci Model Dev 2019, 12, 4681–4703, doi:10.5194/gmd-12-4681-2019.
21. Hantson, S.; Arneth, A.; Harrison, S.P.; Kelley, D.I.; Colin Prentice, I.; Rabin, S.S.; Archibald, S.; Mouillot, F.; Arnold, S.R.; Artaxo, P.; et al. The Status and Challenge of Global Fire Modelling. Biogeosciences 2016, 13, doi:10.5194/bg-13-3359-2016.
22. Laurent, P.; Mouillot, F.; Yue, C.; Ciais, P.; Moreno, M.V.; Nogueira, J.M.P. FRY, a Global Database of Fire Patch Functional Traits Derived from Space-Borne Burned Area Products. Sci Data 2018, 5, doi:10.1038/sdata.2018.132.
23. Lizundia-Loiola, J.; Otón, G.; Ramo, R.; Chuvieco, E. A Spatio-Temporal Active-Fire Clustering Approach for Global Burned Area Mapping at 250 m from MODIS Data. Remote Sens Environ 2020, 236, 111493, doi:https://doi.org/10.1016/j.rse.2019.111493.
24. Otón, G.; Lizundia-Loiola, J.; Pettinari, M.L.; Chuvieco, E. Development of a Consistent Global Long-Term Burned Area Product (1982–2018) Based on AVHRR-LTDR Data. International Journal of Applied Earth Observation and Geoinformation 2021, 103, doi:10.1016/j.jag.2021.102473.
25. Lizundia-Loiola, J.; Franquesa, M.; Khairoun, A.; Chuvieco, E. Global Burned Area Mapping from Sentinel-3 Synergy and VIIRS Active Fires. Remote Sens Environ 2022, 282, 113298, doi:https://doi.org/10.1016/j.rse.2022.113298.
26. Chuvieco, E.; Roteta, E.; Sali, M.; Stroppiana, D.; Boettcher, M.; Kirches, G.; Storm, T.; Khairoun, A.; Pettinari, M.L.; Franquesa, M.; et al. Building a Small Fire Database for Sub-Saharan Africa from Sentinel-2 High-Resolution Images. Science of the Total Environment 2022, 845, doi:10.1016/j.scitotenv.2022.157139.
27. Roteta, E.; Bastarrika, A.; Padilla, M.; Storm, T.; Chuvieco, E. Development of a Sentinel-2 Burned Area Algorithm: Generation of a Small Fire Database for Sub-Saharan Africa. Remote Sens Environ 2019, 222, 1–17, doi:10.1016/j.rse.2018.12.011.
28. Giglio, L.; Boschetti, L.; Roy, D.P.; Humber, M.L.; Justice, C.O. The Collection 6 MODIS Burned Area Mapping Algorithm and Product. Remote Sens Environ 2018, 217, 72–85, doi:10.1016/j.rse.2018.08.005.

29. Lizundia-Loiola, J.; Franquesa, M.; Boettcher, M.; Kirches, G.; Pettinari, M.L.; Chuvieco, E. Implementation of the Burned Area Component of the Copernicus Climate Change Service: From Modis to Olci Data. Remote Sens (Basel) 2021, 13, doi:10.3390/rs13214295.
30. San-Miguel-Ayanz, J.; Schulte, E.; Schmuck, G.; Camia, A.; Strobl, P.; Liberta, G.; Giovando, C.; Boca, R.; Sedano, F.; Kempeneers, P. Comprehensive Monitoring of Wildfires in Europe: The European Forest Fire Information System (EFFIS). In Approaches to managing disaster-Assessing hazards, emergencies and disaster impacts; IntechOpen, 2012 ISBN 953510294X.
31. Mouillot, F.; Schultz, M.G.; Yue, C.; Cadule, P.; Tansey, K.; Ciais, P.; Chuvieco, E. Ten Years of Global Burned Area Products from Spaceborne Remote Sensing-A Review: Analysis of User Needs and Recommendations for Future Developments. International Journal of Applied Earth Observation and Geoinformation 2014, 26.
32. Long, T.; Zhang, Z.; He, G.; Jiao, W.; Tang, C.; Wu, B.; Zhang, X.; Wang, G.; Yin, R. 30m Resolution Global Annual Burned Area Mapping Based on Landsat Images and Google Earth Engine. Remote Sens (Basel) 2019, 11, doi:10.3390/rs11050489.
33. Gorelick, N.; Hancher, M.; Dixon, M.; Ilyushchenko, S.; Thau, D.; Moore, R. Google Earth Engine: Planetary-Scale Geospatial Analysis for Everyone. Remote Sens Environ 2017, 202, 18–27, doi:10.1016/j.rse.2017.06.031.
34. Eidenshink, J.; Schwind, B.; Brewer, K.; Zhu, Z.-L.; Quayle, B.; Howard, S. A Project for Monitoring Trends in Burn Severity. Fire Ecology 2007, 3, doi:10.4996/fireecology.0301003.
35. Hawbaker, T.J.; Vanderhoof, M.K.; Schmidt, G.L.; Beal, Y.J.; Picotte, J.J.; Takacs, J.D.; Falgout, J.T.; Dwyer, J.L. The Landsat Burned Area Algorithm and Products for the Conterminous United States. Remote Sens Environ 2020, 244, doi:10.1016/j.rse.2020.111801.
36. Ramo, R.; Roteta, E.; Bistinas, I.; van Wees, D.; Bastarrika, A.; Chuvieco, E.; van der Werf, G.R. African Burned Area and Fire Carbon Emissions Are Strongly Impacted by Small Fires Undetected by Coarse Resolution Satellite Data. Proc Natl Acad Sci U S A 2021, 118, doi:10.1073/pnas.2011160118.
37. Khairoun, A.; Mouillot, F.; Chen, W.; Ciais, P.; Chuvieco, E. Coarse-Resolution Burned Area Datasets Severely Underestimate Fire-Related Forest Loss. Science of The Total Environment 2024, 170599.
38. Katagis, T.; Gitas, I.Z. Assessing the Accuracy of MODIS MCD64A1 C6 and FireCCI51 Burned Area Products in Mediterranean Ecosystems. Remote Sens (Basel) 2022, 14, doi:10.3390/rs14030602.
39. Liu, J.; Heiskanen, J.; Maeda, E.E.; Pellikka, P.K.E. Burned Area Detection Based on Landsat Time Series in Savannas of Southern Burkina Faso. International Journal of Applied Earth Observation and Geoinformation 2018, 64, doi:10.1016/j.jag.2017.09.011.
40. Llorens, R.; Sobrino, J.A.; Fernández, C.; Fernández-Alonso, J.M.; Vega, J.A. A Methodology to Estimate Forest Fires Burned Areas and Burn Severity Degrees Using Sentinel-2 Data. Application to the October 2017 Fires in the Iberian Peninsula. International Journal of Applied Earth Observation and Geoinformation 2021, 95, doi:10.1016/j.jag.2020.102243.
41. Gaveau, D.L.A.; Descals, A.; Salim, M.A.; Sheil, D.; Sloan, S. Refined Burned-Area Mapping Protocol Using Sentinel-2 Data Increases Estimate of 2019 Indonesian Burning. Earth Syst Sci Data 2021, 13, doi:10.5194/essd-13-5353-2021.
42. Roteta, E.; Bastarrika, A.; Franquesa, M.; Chuvieco, E. Landsat and Sentinel-2 Based Burned Area Mapping Tools in Google Earth Engine. Remote Sens (Basel) 2021, 13, 1–30, doi:10.3390/rs13040816.
43. Fernández-García, V.; Franquesa, M.; Kull, C.A. Madagascar's Burned Area from Sentinel-2 Imagery (2016–2022): Four Times Higher than from Lower Resolution Sensors. Science of The Total Environment 2024, 169929.
44. Oliva, P.; Mansilla, R.; Roteta, E.; Pérez-Martínez, W. Suitability of Band Angle Indices for Burned Area Mapping in the Maule Region (Chile). Frontiers in Forests and Global Change 2023, 5, doi:10.3389/ffgc.2022.1052299.
45. Stroppiana, D.; Sali, M.; Busetto, L.; Boschetti, M.; Ranghetti, L.; Franquesa, M.; Pettinari, M.L.; Chuvieco, E. Sentinel-2 Sampling Design and Reference Fire Perimeters to Assess Accuracy of Burned Area Products over Sub-Saharan Africa for the Year 2019. ISPRS Journal of Photogrammetry and Remote Sensing 2022, 191, doi:10.1016/j.isprsjprs.2022.07.015.
46. Roteta, E.; Bastarrika, A.; Ibisate, A.; Chuvieco, E. A Preliminary Global Automatic Burned-Area Algorithm at Medium Resolution in Google Earth Engine. Remote Sens (Basel) 2021, 13, doi:10.3390/rs13214298.

47. Chuvieco, E.; Yebra, M.; Martino, S.; Thonicke, K.; Gómez-Giménez, M.; San-Miguel, J.; Oom, D.; Velea, R.; Mouillot, F.; Molina, J.R.; et al. Towards an Integrated Approach to Wildfire Risk Assessment: When, Where, What and How May the Landscapes Burn. Fire 2023, 6, doi:10.3390/fire6050215.
48. Véla, E.; Benhouhou, S. Évaluation d'un Nouveau Point Chaud de Biodiversité Végétale Dans Le Bassin Méditerranéen (Afrique Du Nord). C R Biol 2007, 330, doi:10.1016/j.crvi.2007.04.006.
49. UNESCO Biosphere Reserves in Arab States Available online: https://en.unesco.org/biosphere/arab-states (accessed on 1 November 2023).
50. FAO-DGF Plan National de Gestion Des Incendies de Forêt Algérie 2021-2030; 2022;
51. Meddour-Sahar, O.; Derridj, A. Bilan Des Feux de Forêts En Algérie : Analyse Spatio-Temporelle et Cartographie Du Risque (Période 1985-2010). Science et Changements Planetaires - Secheresse 2012, 23, doi:10.1684/sec.2012.0342.
52. Zanaga, D.; Van De Kerchove, R.; Daems, D.; De Keersmaecker, W.; Brockmann, C.; Kirches, G.; Wevers, J.; Cartus, O.; Santoro, M.; Fritz, S. ESA WorldCover 10 m 2021 V200. 2022, doi:https://doi.org/10.5281/zenodo.7254221.
53. USGS USGS EROS Archive - Digital Elevation - Shuttle Radar Topography Mission (SRTM) 1 Arc-Second Global Available online: https://www.usgs.gov/centers/eros/science/usgs-eros-archive-digital-elevation-shuttle-radar-topography-mission-srtm-1?qt-science_center_objects=0#qt-science_center_objects.
54. Wulder, M.A.; Roy, D.P.; Radeloff, V.C.; Loveland, T.R.; Anderson, M.C.; Johnson, D.M.; Healey, S.; Zhu, Z.; Scambos, T.A.; Pahlevan, N.; et al. Fifty Years of Landsat Science and Impacts. Remote Sens Environ 2022, 280.
55. USGS Landsat Missions Available online: https://www.usgs.gov/landsat-missions (accessed on 14 July 2023).
56. European Space Agency SENTINEL-2 User Handbook. Sentinel-2 User Handbook 2015.
57. Giglio, L.; Schroeder, W.; Justice, C.O. The Collection 6 MODIS Active Fire Detection Algorithm and Fire Products. Remote Sens Environ 2016, 178, doi:10.1016/j.rse.2016.02.054.
58. Schroeder, W.; Oliva, P.; Giglio, L.; Csiszar, I.A. The New VIIRS 375m Active Fire Detection Data Product: Algorithm Description and Initial Assessment. Remote Sens Environ 2014, 143, doi:10.1016/j.rse.2013.12.008.
59. Turco, M.; Llasat, M.C.; Tudela, A.; Castro, X.; Provenzale, A. Decreasing Fires in a Mediterranean Region (1970-2010, NE Spain). Natural Hazards and Earth System Science 2013, 13, doi:10.5194/nhess-13-649-2013.
60. Ruffault, J.; Mouillot, F. How a New Fire-suppression Policy Can Abruptly Reshape the Fire-weather Relationship. Ecosphere 2015, 6, 1–19.
61. Bastarrika, A.; Alvarado, M.; Artano, K.; Martinez, M.P.; Mesanza, A.; Torre, L.; Ramo, R.; Chuvieco, E. BAMS: A Tool for Supervised Burned Area Mapping Using Landsat Data. Remote Sens (Basel) 2014, 6, 12360–12380, doi:10.3390/rs61212360.
62. Bastarrika, A.; Chuvieco, E.; Martín, M.P. Mapping Burned Areas from Landsat TM/ETM+ Data with a Two-Phase Algorithm: Balancing Omission and Commission Errors. Remote Sens Environ 2011, 115, 1003–1012, doi:10.1016/j.rse.2010.12.005.
63. Alonso-Canas, I.; Chuvieco, E. Global Burned Area Mapping from ENVISAT-MERIS and MODIS Active Fire Data. Remote Sens Environ 2015, 163, 140–152, doi:10.1016/j.rse.2015.03.011.
64. Chuvieco, E.; Lizundia-Loiola, J.; Pettinari, M.L.; Ramo, R.; Padilla, M.; Tansey, K.; Mouillot, F.; Laurent, P.; Storm, T.; Heil, A. Generation and Analysis of a New Global Burned Area Product Based on MODIS 250 m Reflectance Bands and Thermal Anomalies. Earth Syst Sci Data 2018, 10, 2015–2031, doi:https://doi.org/10.5194/essd-10-2015-2018.
65. Vanderhoof, M.K.; Fairaux, N.; Beal, Y.J.G.; Hawbaker, T.J. Validation of the USGS Landsat Burned Area Essential Climate Variable (BAECV) across the Conterminous United States. Remote Sens Environ 2017, 198, 393–406, doi:10.1016/j.rse.2017.06.025.
66. Pleniou, M.; Xystrakis, F.; Dimopoulos, P.; Koutsias, N. Maps of Fire Occurrence - Spatially Explicit Reconstruction of Recent Fire History Using Satellite Remote Sensing. J Maps 2012, 8, 499–506, doi:10.1080/17445647.2012.743866.
67. Argañaraz, J.P.; Pizarro, G.G.; Zak, M.; Bellis, L.M. Fire Regime, Climate, and Vegetation in the Sierras de Córdoba, Argentina. Fire Ecology 2015, 11, 55–73, doi:10.4996/fireecology.1101055.
68. Breiman, L. Random Forests. Mach Learn 2001, 45, doi:10.1023/A:1010933404324.

69. Rouse, J.W.; Haas, R.H.; Schell, J.A.; Deering, D.W. Monitoring Vegetation Systems in the Great Plains with ERTS. NASA Special Publication. NASA special publication 1974, 24.
70. Key, C.H.; Benson, N.C. The Normalized Burn Ratio (NBR): A Landsat TM Radiometric Measure of Burn Severity. United States Geological Survey, Northern Rocky Mountain Science Center: Bozeman, MT, USA 1999.
71. García, M.J.L.; Caselles, V. Mapping Burns and Natural Reforestation Using Thematic Mapper Data. Geocarto Int 1991, 6, 31–37, doi:https://doi.org/10.1080/10106049109354290.
72. Justice, C.; Belward, A.; Morisette, J.; Lewis, P.; Privette, J.; Baret, F. Developments in the "validation" of Satellite Sensor Products for the Study of the Land Surface. Int J Remote Sens 2000, 21, doi:10.1080/014311600750020000.
73. Boschetti, L.; Stehman, S. V.; Roy, D.P. A Stratified Random Sampling Design in Space and Time for Regional to Global Scale Burned Area Product Validation. Remote Sens Environ 2016, 186, doi:10.1016/j.rse.2016.09.016.
74. Padilla, M.; Olofsson, P.; Stehman, S. V.; Tansey, K.; Chuvieco, E. Stratification and Sample Allocation for Reference Burned Area Data. Remote Sens Environ 2017, 203, doi:10.1016/j.rse.2017.06.041.
75. Olson, D.M.; Dinerstein, E.; Wikramanayake, E.D.; Burgess, N.D.; Powell, G.V.N.; Underwood, E.C.; D'amico, J.A.; Itoua, I.; Strand, H.E.; Morrison, J.C.; et al. Terrestrial Ecoregions of the World: A New Map of Life on Earth: A New Global Map of Terrestrial Ecoregions Provides an Innovative Tool for Conserving Biodiversity. Bioscience 2001, 51, doi:https://doi.org/10.1641/0006-3568(2001)051[0933:TEOTWA]2.0.CO;2.
76. Franquesa, M.; Vanderhoof, M.K.; Stavrakoudis, D.; Gitas, I.Z.; Roteta, E.; Padilla, M.; Chuvieco, E. Development of a Standard Database of Reference Sites for Validating Global Burned Area Products. Earth Syst Sci Data 2020, 12, 3229–3246, doi:10.5194/essd-12-3229-2020.
77. Franquesa, M.; Rodriguez-Montellano, A.M.; Chuvieco, E.; Aguado, I. Reference Data Accuracy Impacts Burned Area Product Validation: The Role of the Expert Analyst. Remote Sens (Basel) 2022, 14, doi:10.3390/rs14174354.
78. Boschetti, L.; Roy, D.P.; Justice, C.O. International Global Burned Area Satellite Product Validation Protocol. Part I–Production and Standardization of Validation Reference Data. Committee on Earth Observation Satellites: Maryland, MD, USA 2009, 1–11.
79. Franquesa, M.; Lizundia-Loiola, J.; Stehman, S. V.; Chuvieco, E. Using Long Temporal Reference Units to Assess the Spatial Accuracy of Global Satellite-Derived Burned Area Products. Remote Sens Environ 2022, 269, doi:10.1016/j.rse.2021.112823.
80. Dice, L.R. Measures of the Amount of Ecologic Association Between Species. Ecology 1945, 26, doi:10.2307/1932409.
81. Congalton, R.G.; Green, K. Assessing the Accuracy of Remotely Sensed Data: Principles and Practices; CRC press, 2019; ISBN 0429629354.
82. Padilla, M.; Wheeler, J.; Tansey, K. ESA CCI ECV Fire Disturbance: D4. 1.1 Product Validation Report, Version 2.1. Tech. Rep. 2018.
83. Giglio, L.; Schroeder, W.; Hall, J. V; Justice, C.O. MODIS Collection 6 Active Fire Product User's Guide Revision C 2020.
84. Peterson, B.G.; Carl, P.; Boudt, K.; Bennett, R.; Ulrich, J.; Zivot, E.; Cornilly, D.; Hung, E.; Lestel, M.; Balkissoon, K. Package 'Performanceanalytics.' R Team Cooperation 2018, 3, 13–14.
85. Kendall, M.G. Rank Correlation Methods. Biometrika 1957, 44, doi:10.2307/2333282.
86. Mann, H.B. Nonparametric Tests Against Trend. Econometrica 1945, 13, doi:10.2307/1907187.
87. Sen, P.K. Estimates of the Regression Coefficient Based on Kendall's Tau. J Am Stat Assoc 1968, 63, doi:10.1080/01621459.1968.10480934.
88. Otón, G.; Pereira, J.M.C.; Silva, J.M.N.; Chuvieco, E. Analysis of Trends in the Firecci Global Long Term Burned Area Product (1982–2018). Fire 2021, 4, doi:10.3390/fire4040074.
89. Ricotta, C.; Arianoutsou, M.; Díaz-Delgado, R.; Duguy, B.; Lloret, F.; Maroudi, E.; Mazzoleni, S.; Manuel Moreno, J.; Rambal, S.; Vallejo, R.; et al. Self-Organized Criticality of Wildfires Ecologically Revisited. Ecol Modell 2001, 141.
90. Padilla, M.; Stehman, S. V.; Ramo, R.; Corti, D.; Hantson, S.; Oliva, P.; Alonso-Canas, I.; Bradley, A. V.; Tansey, K.; Mota, B.; et al. Comparing the Accuracies of Remote Sensing Global Burned Area Products Using Stratified Random Sampling and Estimation. Remote Sens Environ 2015, 160, 114–121, doi:10.1016/j.rse.2015.01.005.

91. Achour, H.; Toujani, A.; Trabelsi, H.; Jaouadi, W. Evaluation and Comparison of Sentinel-2 MSI, Landsat 8 OLI, and EFFIS Data for Forest Fires Mapping. Illustrations from the Summer 2017 Fires in Tunisia. Geocarto Int 2021, doi:10.1080/10106049.2021.1980118.
92. Vallet, L.; Schwartz, M.; Ciais, P.; van Wees, D.; de Truchis, A.; Mouillot, F. High-Resolution Data Reveal a Surge of Biomass Loss from Temperate and Atlantic Pine Forests, Contextualizing the 2022 Fire Season Distinctiveness in France. Biogeosciences 2023, 20, 3803–3825.
93. Storey, J.C.; Choate, M.J. Landsat-5 Bumper-Mode Geometric Correction. IEEE Transactions on Geoscience and Remote Sensing 2004, 42.
94. Turco, M.; Jerez, S.; Augusto, S.; Tarín-Carrasco, P.; Ratola, N.; Jiménez-Guerrero, P.; Trigo, R.M. Climate Drivers of the 2017 Devastating Fires in Portugal. Sci Rep 2019, 9, doi:10.1038/s41598-019-50281-2.
95. Chergui, B.; Fahd, S.; Santos, X.; Pausas, J.G. Socioeconomic Factors Drive Fire-Regime Variability in the Mediterranean Basin. Ecosystems 2018, 21, doi:10.1007/s10021-017-0172-6.
96. Bajocco, S.; Ferrara, C.; Guglietta, D.; Ricotta, C. Easy-to-Interpret Procedure to Analyze Fire Seasonality and the Influence of Land Use in Fire Occurrence: A Case Study in Central Italy. Fire 2020, 3.
97. Michetti, M.; Pinar, M. Forest Fires Across Italian Regions and Implications for Climate Change: A Panel Data Analysis. Environ Resour Econ (Dordr) 2019, 72, doi:10.1007/s10640-018-0279-z.
98. Salvati, L.; Ranalli, F. "Land of Fires": Urban Growth, Economic Crisis, and Forest Fires in Attica, Greece. Geographical Research 2015, 53, doi:10.1111/1745-5871.12093.
99. Nojarov, P.; Nikolova, M. Heat Waves and Forest Fires in Bulgaria. Natural Hazards 2022, 114, doi:10.1007/s11069-022-05451-3.
100. Calheiros, T.; Nunes, J.P.; Pereira, M.G. Recent Evolution of Spatial and Temporal Patterns of Burnt Areas and Fire Weather Risk in the Iberian Peninsula. Agric For Meteorol 2020, 287, doi:10.1016/j.agrformet.2020.107923.
101. Turco, M.; Bedia, J.; Di Liberto, F.; Fiorucci, P.; Von Hardenberg, J.; Koutsias, N.; Llasat, M.C.; Xystrakis, F.; Provenzale, A. Decreasing Fires in Mediterranean Europe. PLoS One 2016, 11, doi:10.1371/journal.pone.0150663.
102. Pausas, J.G. Changes in Fire and Climate in the Eastern Iberian Peninsula (Mediterranean Basin). Clim Change 2004, 63, doi:10.1023/B:CLIM.0000018508.94901.9c.
103. Chriha, S.; Sghari, A. Les Incendies de Forêt En Tunisie. Séquelles Irréversibles de La Révolution de 2011. Méditerranée. Revue géographique des pays méditerranéens/Journal of Mediterranean geography 2013, 87–93.
104. Lemus-Canovas, M.; Insua-Costa, D.; Trigo, R.M.; Miralles, D.G. Record-Shattering 2023 Spring Heatwave in Western Mediterranean Amplified by Long-Term Drought. NPJ Clim Atmos Sci 2024, 7, 25.
105. Bastarrika, A.; Chuvieco, E.; Martin, M.P. Automatic Burned Land Mapping from MODIS Time Series Images: Assessment in Mediterranean Ecosystems. In Proceedings of the IEEE Transactions on Geoscience and Remote Sensing; 2011; Vol. 49.
106. Hall, J. V.; Zibtsev, S. V.; Giglio, L.; Skakun, S.; Myroniuk, V.; Zhuravel, O.; Goldammer, J.G.; Kussul, N. Environmental and Political Implications of Underestimated Cropland Burning in Ukraine. Environmental Research Letters 2021, 16, doi:10.1088/1748-9326/abfc04.mer/
107. Kouachi, M. E., Khairoun, A., Baeza, M., & Moutahir, H. (2024). 40-year fire history reconstruction from Landsat data in Mediterranean ecosystems of Algeria (1984–2023) (1.0) [Data set]. Zenodo. https://doi.org/10.5281/zenodo.10680088